



Joint European Research Infrastructure network for Coastal Observatory – Novel European eXpertise for coastal observaTories - <b>JERICO-NEXT</b>	
<b>Deliverable title</b>	Report on final assessment of methodological improvements and testing.
<b>Work Package Title</b>	WP 3 Innovations in Technology and Methodology
<b>Deliverable number</b>	D3.4
<b>Description</b>	Development and testing of methodological improvements on JERICO-NEXT infrastructures.
<b>Lead beneficiary</b>	
<b>Lead Authors</b>	Annalisa Griffa (CNR-ISMAR), Jochen Horstmann (HZG), Julien Mader (AZTI), Anna Rubio (AZTI), Maristella Berta (CNR-ISMAR), Alejandro Orfila (IMEDEA-UIB-CSIC), Lars Axell (SMHI)
<b>Contributors</b>	Ainhoa Caballero (AZTI), Guillaume Charria (IFREMER), Lorenzo Corgnati (CNR-ISMAR), Pierre De Mey (CNRS), Erick Fredj (Univ. Jerusalem), Ismael Hernandez-Carrasco (UIB-CSIC), Gabriel Jordà (IEO), Ivan Manso (AZTI), Carlo Mantovani (CNR-ISMAR), Celine Quentin (MIO-CNRS), Emma Reyes (SOCIB), Jose German Rodriguez (AZTI), Lohitzune Solabarrieta(KAUST)
<b>Submitted by</b>	Annalisa Griffa
<b>Revision number</b>	V2





<b>Revision Date</b>	18/07/2019
<b>Security</b>	Consortium Only or Public

<b>History</b>			
<b>Revision</b>	<b>Date</b>	<b>Modification</b>	<b>Author</b>
1	10/06/2019	Initial version	A. Griffa
2	18/07/2019	Update after WP lead review	A. Griffa

<b>Approvals</b>				
	<b>Name</b>	<b>Organisation</b>	<b>Date</b>	<b>Visa</b>
<b>Coordinator</b>	Patrick Farcy	Ifremer	09/08/2019	PF
<b>WP Leaders</b>	George Petihakis Laurent Delauney	HCMR Ifremer	17/07/2019	

**PROPRIETARY RIGHTS STATEMENT**

THIS DOCUMENT CONTAINS INFORMATION, WHICH IS PROPRIETARY TO THE **JERICO-NEXT** CONSORTIUM. NEITHER THIS DOCUMENT NOR THE INFORMATION CONTAINED HEREIN SHALL BE USED, DUPLICATED OR COMMUNICATED EXCEPT WITH THE PRIOR WRITTEN CONSENT OF THE **JERICO-NEXT** COORDINATOR.





---

## Table of contents

1. Executive Summary .....	4
2. Introduction .....	6
3. Main report.....	8
4. Conclusions .....	51
5. Annexes and references .....	54





## 1. Executive Summary

Deliverable D3.4 is the second and final deliverable of Task 3.2, where a final assessment and testing of all the new developed methodologies related to HF radar data is provided. An impressive suite of new tools is presented, and their impact on the use of HF radars is discussed. HF radars are today a vital and growing part of the observing system in Europe, and Task 3.2, have greatly contributed to this growth through methodological development. The work has been performed in synergy with other WPs, in particular WP4 for testing in specific areas, and WP5 for the elaboration of interoperability standards. Scientific collaborations have included a number of international scientists and institutions also outside the original JERICO-NEXT consortium, Testing has been carried out using data from several installations in various European seas and oceans, including the German Bight, the Bay of Biscay, the West Med, the Adriatic Sea and the Swedish coasts.

The developments focus on the following three main aspects, mirroring the three subtasks in Task 3.2: 1) scientific basis for quality control and interoperability standards; 2) methods to optimize installation planning; 3) methods for advanced analyses to be used in practical applications.

1. The quality of current retrievals has been investigated, and methods to improve their QC have been developed and tested. A focused scientific investigation has been performed on how to quantify accuracy in the important and challenging case of high current sub-grid variability. The approach, tested in the German Bight, provides general methodological indications that can be applied to different situations. Also, scientific support has been provided to the interoperability effort carried out in the framework of WP5. Improved recommendations for European QC have been investigated thanks to an international collaboration, providing the basis for the results in the WP5 deliverable D5.14.
2. Methods to guide the design of HF radar networks have been completed. A cost benefit analysis is made available taking into account the geographical distribution of the requirements and the geographical capabilities of the existing and potential HF radar network. It allows the prioritization of potential new platforms considering their respective contribution into the overall impact of the HF Radar network. As a demonstrator, different scenarios have been assessed for the development of long-range HF Radar network in the Bay of Biscay and north-western Iberian Peninsula. An additional tool has been introduced for considering the variability of the ocean processes at the scale resolved by the targeted observing platform.





3. A number of new products have been implemented for the analyses of HF radar data and their use in practical applications. Methods for blending HF radar data with water column information from ADCP and glider data have been implemented and tested, providing guidance for important future applications toward the integration of different observing system components. Various gap filling methods have been tested and a new one implemented, in order to ensure smooth trajectory computations for transport applications. Innovative flow characterization methods for biological applications have been explored. They include Lagrangian methods to quantify flow transport and retention, and their impact on phytoplankton or larval transport and fishery management, as well as a new class of indexes of small scale divergence and vertical velocities with potential ecosystem impact. Finally, two different approaches to improve transport and flow forecasting using HF radar data have been assessed.





## 2. Introduction

In the framework of JERICO-NEXT, a significant body of research has been dedicated to data retrieval and analysis for High Frequency (HF) coastal radars, with the overarching goal of improving emerging technologies that are part of the core observing system of Europe's coastal seas and oceans. HF radars are very powerful instruments, providing information on surface velocity in terms of hourly maps over extended regions (range up to 100 km) and with high spatial resolution (order of 1-3 km). This information can be used to address several societal needs such as navigation safety, search and rescue, oil spill or other pollutant tracking, marine protected area and fishery management.

The challenge that motivated the research performed in Task 3.2 (WP3) is to produce innovative methodologies that can optimize the usability of HF radar data. This general goal has many aspects and aims at providing a) scientific basis for quality control and interoperability standards; b) methods to optimize installation planning; c) methods for advanced analyses to be used in practical applications.

Deliverable D3.4 is the second and final deliverable of Task 3.2. In the previous deliverable, D3.3, a first report was provided on methodological improvements focused on the first two aspects above. In D3.4 a final assessment and testing of all the new methodologies is provided. Testing has been carried out using data from several installations in various European seas and oceans, including the German Bight, the Bay of Biscay, the West Mediterranean Sea, the Adriatic Sea and the Swedish coasts.

The work has been performed in synergy with other WPs, in particular WP4 for tests in specific areas and for specific thematic, and WP5 for the elaboration of interoperability standards. Scientific collaborations have included also scientists and institutions that were not part of the original JERICO-NEXT consortium, as acknowledged in the text.

The main results of D3.4 are presented in Section 3, which is organized in 3 sections that mirror the 3 subtasks of Task 3.2.

Section 3.1 presents the final results of subtask 3.2.1, "New HF radar procedures for current retrievals and quality control", and has two main threads. One thread focuses on methods to quantify the accuracy of velocity data in the challenging case of high variability in the current field that is not fully resolved by the HF radar measurements. Initial results were provided in D3.3, while here a complete investigation of the accuracy parameter and threshold are provided. The other thread deals with interoperability, and in D3.3 investigations were reported regarding improved QC





(Quality Control) tests suggested on the basis of the first recommendation provided by WP5 in D5.13. Here the actual transition of the scientific tests toward operability and inclusion in the final recommendation D5.14 are reported.

Section 3.2 presents results from Subtask 3.2.2 “HF Radar network development”. In D3.3 the link between the societal needs and the role of the HF radar network has been described. Then a methodology to consider the impact of the operating frequency and sites locations and some numerical tools for integrating the ocean phenomena distribution have been presented. Here the application of this methodology to assess different scenarios of installation planning for the HF radar network in a pilot area is reported.

Finally Section 3.3 reports on results from subtask 3.3.3 “New products for 4d characterization of shelf/slope hydrodynamics and transport”, that was not included in D3.3. Several results are presented, expanding on several different methodological tools that enhance HF radar data value not only for scientific purposes but also for societal needs and applications. The tools include: data blending with water column measurements, gap filling, transport applications and improvement of forecasting capabilities.





### 3. Main report

#### 3.1 New HF radar procedures for current retrievals and data Quality control (Subtask 3.2.1, Leader HZG)

In this subsection, new results from Subtask 3.2.1 are reported, that were not included in D3.3. The performed work focuses mostly on the assessment and testing of new methods for HF radar current retrievals in presence of high variability (3.1.1), and on the transition of research results toward final recommendations for common protocols (3.1.2).

##### 3.1.1 Improvements of Algorithms for HF-Radar Data in Presence of Complex Bathymetry and Current Variability, and Associated Quality Control (HZG)

In the report D 3.3 within subtask 3.2.1 we have described a method to remove radar frequency interferences and ship echoes within HF-radar data from phased array systems. Furthermore, we have analysed HF-radar retrieved surface current errors due to sub-resolution changes of currents utilizing the data of the German HF-radar network. In addition, we have developed an approach to reduce surface current errors by temporal backtracking of HF-radar retrieved current data.

Within this report, the current accuracy parameter provided by the WERA software, is inspected with respect to its suitability to identify HF-radar retrieved surface current errors induced by sub-resolution changes of currents. The validity of the current accuracy parameter is evaluated and tested investigating HF-radar data from Büsum (German Bight) as well as numerical model data from the Federal Maritime and Hydrographic Agency of Germany. Last but not least a threshold parameter is derived to extract all HF-radar data, which are possibly affected by sub-resolution changes of currents.

##### 3.1.1.1 Definition of the Accuracy Parameter

The variation of surface currents within a resolution cell as well as during the integration time of a HF-radar measurement leads to a broadening of the first-order Bragg lines in the Doppler spectra. Within this deliverable, we will introduce and test a parameter to improve the quality control to identify surface current errors due to sub-resolution changes of currents or bathymetry utilizing the data of the German HF-radar network. Within the WERA software (utilized within the German HF-radar network for surface current retrieval), the bandwidth of the first order Bragg lines is retrieved and an accuracy parameter which is derived from this magnitude is provided. In this report, it will be shown that the accuracy parameter is a very good estimate for the spatial sub resolution variation of a HF-radar current.

Due to the high importance of the inhomogeneities in the coastal waters of the German Bight we have investigated the behaviour and shape of the first order Doppler peaks in time and space under inhomogeneous and homogeneous



situations as well as under different tidal phases and optimized the accuracy estimations under these complex situations.

A HF-radar measurement of radial velocity consists of several samples (chirps). For each sample  $i$ , the radial velocity  $v$  and signal to noise ratio SNR is calculated. The mean velocity over the measurement is the SNR-weighted velocity of samples:

$$\langle v \rangle_{SNR} = \frac{\sum_{i=1}^N v_i SNR_i}{\sum_{i=1}^N SNR_i}$$

Assuming mutually independent samples the variance  $\sigma^2_{SNR}$  and accuracy parameter  $a_v$  are given by:

$$\sigma^2_{SNR} = \langle v^2 \rangle_{SNR} - \langle v \rangle_{SNR}^2$$

$$a_v = \frac{\langle \sigma \rangle_{SNR}}{\sqrt{N}}$$

A higher variance leads to a broader Bragg-scattering, while a lower variance to a smaller.

### 3.1.1.2 Analyses of the Accuracy Parameter

The factors influencing the accuracy are analyzed with a continuous set of 777 HF-radar measurements from the radar station at Büsum, which were acquired between 29. July and 8. August, 2017. The time difference between consecutive measurements is 20 minutes and the integration time of each measurement consist of 10 minutes of radar data. In Figure 1 the temporal mean (left hand side) and standard deviation (right hand side) of the accuracy parameter from the HF-radar station located at Büsum, German Bight is plotted.

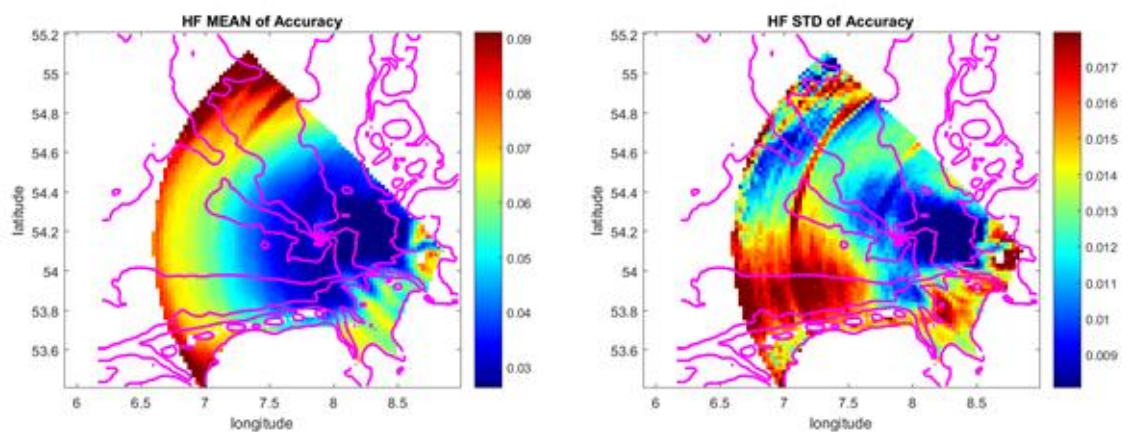


Figure 1: Temporal mean (left hand side) and standard deviation (right hand side) of the accuracy parameter from the HF-radar station located at Büsum, German Bight. The data were acquired between 29. July 2017 and 8. August 2017.

According to the mean accuracy parameter (Figure 1 left hand side) the Bragg lines show the tendency to be broader in the far range as well as near to the



coast. The high value of the accuracy parameters in the far range are due to radar frequency interferences. Data, which cannot be corrected for radar frequency interferences are excluded from this data set. The large accuracy measures in the coastal regions are very likely caused by the modulation of the current in speed and direction on sub radar resolution scales, which is in particular induced by interaction with the seafloor and its strong small-scale variation. The temporal variation over the whole period of analysis is quantified here by the standard deviation of the accuracy parameter (Figure 1 right hand side). The standard deviation is particular large on a circle which is located at a range distance of approximately  $\frac{3}{4}$  of the plotted range as well as in a sector within  $250^\circ$  and  $280^\circ$  versus north. These patterns have a technical origin, and are caused by 50 Hz noise of the alternating current as well as radar frequency interferences. Unfortunately, the suppression of these interferences (refer to D 3.3) does not always work sufficiently. Since we expect a higher value of the accuracy parameter (higher variance) in areas where the water depth is small enough that the bathymetry-variation within one grid cell is able to modulate the near-surface current (See Figure 1 right hand side) we will compare near-shore areas with far-shore areas. Analyzing the dataset of ten days for one grid cell near and one grid cell far off the coast shows a strong relationship between the accuracy parameter in shallow water and the actual velocity during tidal cycles. During tidal rise and fall, the highest values of the accuracy parameter are observed in shallow water while during high or low tide the values are low. In coastal areas the assumption is that the variation of the accuracy parameter is induced by the strong current variability within a resolution cell, which is dependent on the varying currents due to the tidal cycle. To verify the dependence of the accuracy parameter on the tide-induced currents a Fourier spectral analyses of the radial velocity and accuracy parameter time series is performed.

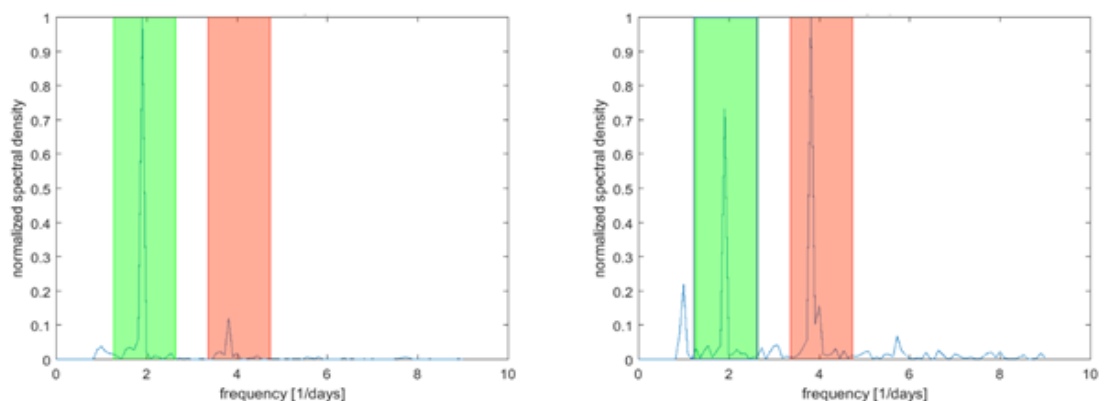


Figure 2: Spectra of radial velocity (left hand side) and accuracy parameter (right hand side) taken from HF-radar data in coastal areas with a tidal current modulated by the bottom topography. The vertical lines indicate the band pass filter to select the fundamental mode (green) and the first harmonic mode (red) of the tidal signal.

In the power spectra of the radial velocity (Figure 2 left hand side), resulting from a time series of a coastal grid cell, most of the energy is located in the fundamental mode of the tidal signal. However, the power spectrum of the

accuracy parameter (Figure 2 right hand side) shows its primary peak at the first harmonic of the tidal signal. This shows the strong tidal cycle dependent changes of the accuracy parameter, most likely caused by current changes on sub-grid cell resolutions of the HF-radar. The harmonic in the accuracy parameter appears because the spatial variation of the surface current is more related to the modulus of the radial current than it's algebraic sign.

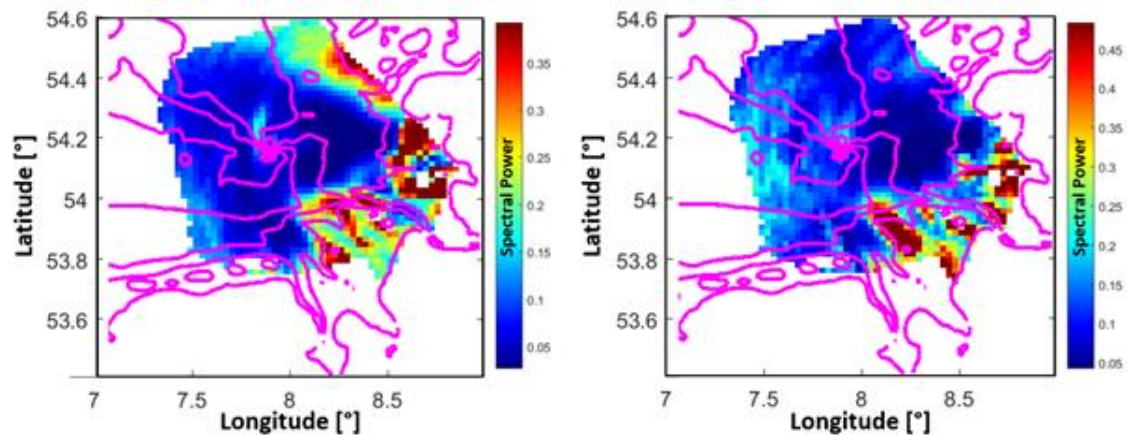


Figure 3: Maps of spectral energy of the frequency spectrum resulting from the accuracy parameter. The map on the left hand side shows the energy belonging to the fundamental mode and the right hand side the energy belonging to the first harmonic of the tidal signal.

In Figure 3 maps of the spectral energy of the accuracy parameter at the frequency of the fundamental mode (left hand side) and the first harmonic mode (right hand side) of the tidal signal are depicted. In case of deep water, the accuracy parameter has no spectral energy at the fundamental mode and the harmonics of the tidal signal, indicating that in deep water the accuracy is not dependent on the tide.

### 3.1.1.3 Current Modulation Parameter

A simple estimation of the variability of current speeds due to the variability of bathymetry in sufficient water depth can be obtained from the equation of continuity, assuming that the influence of spatial variation of the vertical current profile can be neglected. And assuming in addition, that the current velocity along the crest direction of the underwater sand dunes,  $U_{\parallel}$  is constant, the current velocity perpendicular to the sand dunes,  $U_{\perp}$  is governed by the equation of continuity for one dimension:

$$U_{\perp}(x_{\perp}) \cdot d = \text{const},$$

where,  $x_{\perp}$  represents distance along a profile perpendicular to the dune crest and  $d$  the water depth. With respect to the look direction of the radar the spatial gradient is given by

$$\frac{\partial y}{\partial r}(U_r(r)d(r)) = 0,$$

and the radial current velocity modulated by the bottom topography is given by:



$$\frac{1}{U_r} \frac{\partial U_r}{\partial r} = -\frac{s_r}{d(r)}$$

where  $s_r$  is the radial gradient of the water depth. In the following, the parameter  $\frac{s_r}{d(r)} = p_{u,mod}$  is termed as the current modulation parameter because, assuming the validity of the previously stated assumptions, it is directly related the relative spatial gradient of the radial current.

Figure 4 shows a map of the radial current modulation parameter for Büsum considering the same dataset as in in Figure 1. The bathymetry was provided by the operational circulation model BSHcmod [Dick et al., 2001], which has a horizontal resolution of approximately 900 m x 900 m. The spatial gradients were calculated utilizing a sliding filter mask with the length of 5 resolution cells. The standard deviation is calculated for each grid point with its 8 neighbors and finally resampled to the HF-radar grid of around 2000 m x 2000 m resolution using the nearest neighbor method.

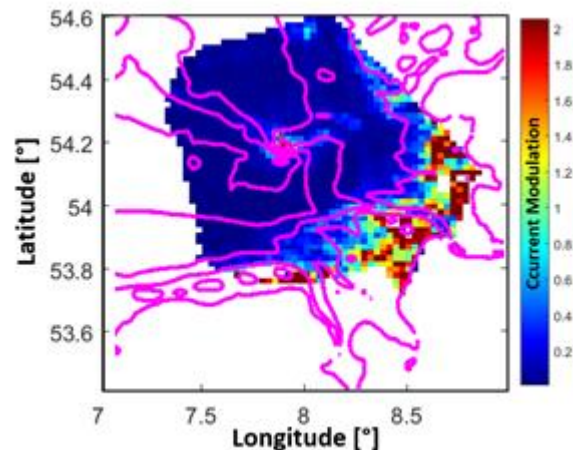


Figure 4: Shows a map of the radial current modulation parameter. This parameter determines the strength of the near-surface horizontal current shear due to the interaction with the variable bottom topography.

### 3.1.1.4 Comparison to Numerical Results

The influence of the variation of sub-grid cell bathymetry on HF-radar measurements was simulated using the data from the operational circulation model BSHcmod. The model uses, instead of a fixed z-grid a generalized vertical coordinate system adjusted to the bathymetry. However, the HF-radar probes the current in the top ~1 m, whereas the top layer of the model represents the current over a varying depth, which is smaller in the shallow waters than in the deeper waters. Accepting this limitation the influence of hydrodynamic interaction of the surface current with the bottom topography is studied as follows: The radial velocity field is calculated by projection of the current vector in the direction of the HF-radar station of Büsum. For the model the accuracy is defined as the standard deviation of the radial velocity, in which the statistical ensemble is defined as the value of one grid cell and its 8 spatial neighbors.

To allow a direct comparison of the HF-radar and the model results the analysis are restricted to the same grid points and time period as of the HF-radar data. Figure 5 depicts the temporal mean and standard deviation of the accuracy parameter derived from the BSHcmod model.

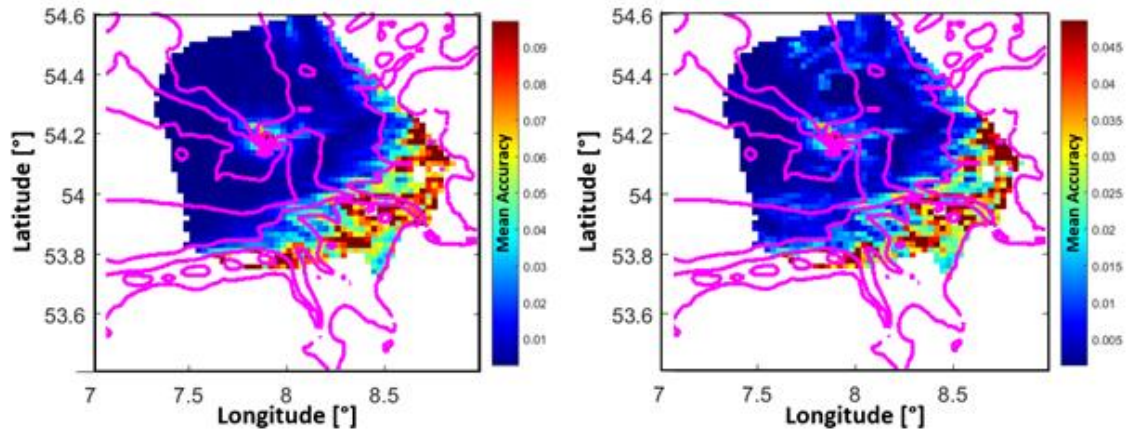


Figure 5: Temporal mean (left) and standard deviation (right) of the accuracy parameter from the BSHcmod model, with selection of the same area and time period as the HF radar station of Büsum.

In contrast to the HF-radar results (Figure 1) the patterns are not affected by technical limitations, e.g. radio frequency interference and range limitations. In coastal areas, as with HR-radar data, the temporal mean and standard deviation of the accuracy parameter is significantly increased.

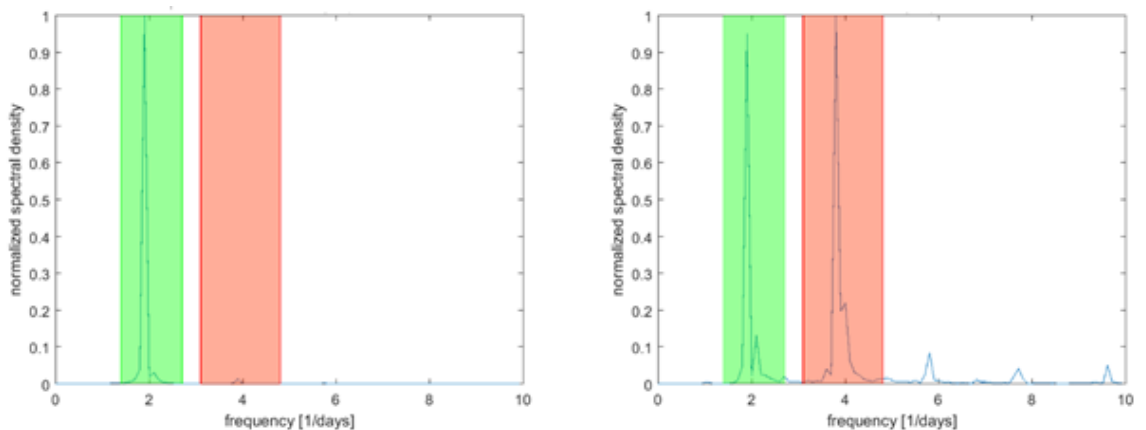


Figure 6: Power spectra of radial velocity (left hand side) and model accuracy (right hand side) taken from the top layer of the BSHcmod model in coastal areas with a tidal current modulated by the bottom topography. The vertical lines indicate the band pass filter to select the fundamental mode (green) and first harmonic mode (red).

To identify the influence of the tidal cycle the power spectrum was calculated for each grid point from the model results. Figure 6 shows the frequency spectrum from a grid point in the coastal area from the radial velocity (left hand side) and accuracy parameter (right hand side). The spectral signal of the velocity is concentrated in the fundamental mode of the tidal signal with only a minor contribution of the first harmonic. In contrast, the spectrum of the accuracy parameter shows a pronounced first harmonic.

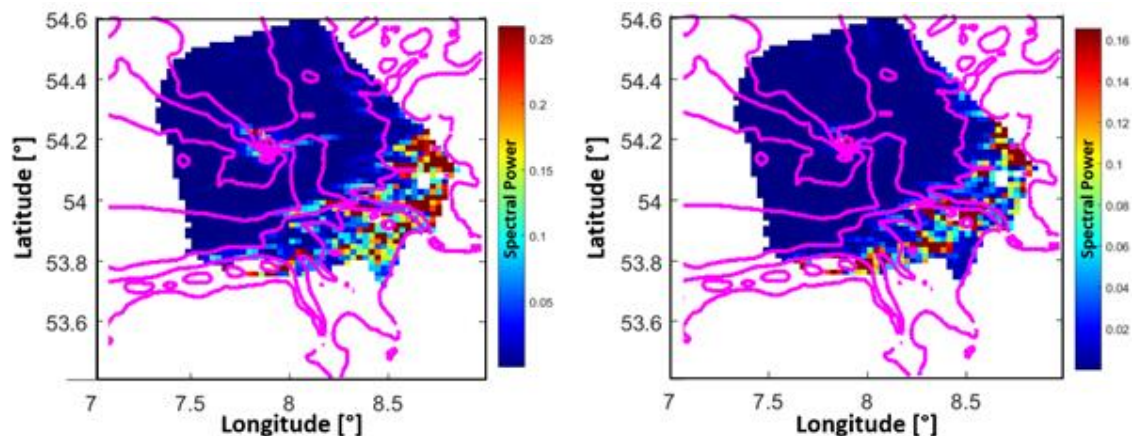


Figure 7: Maps of spectral energy resulting from the numerical model retrieved accuracy frequency spectrum belonging to the fundamental mode (left hand side) and the first harmonic (right hand side) of the tidal signal.

The tidal signal of the velocity spectrum covers the entire area. For the accuracy parameter, it is expected that the fundamental mode and first harmonic mode appear only if the current modulation parameter is high, i.e. in shallow water and for a large bottom slope. The results shown in Figure 7 confirm that the spectral components of the tidal signal of the accuracy parameter are present in coastal areas, in accordance with the HF-radar results shown in Figure 3.

### 3.1.1.5 Estimation of a Threshold for the Accuracy Parameter

As was shown in the previous section both with model results and HF measurements the subscale variation of the HF-radar retrieved radial velocity results in a fundamental mode and first harmonic tidal spectral signature of the time series of the accuracy parameter. Figure 8 presents the histogram of the first harmonic spectral power of the HF-radar accuracy parameter. The histogram is unimodal with a long tail with high spectral power. High power indicates a strong hydrodynamic interaction between the tidal current and the bottom topography on a spatial scale smaller than the HF spatial resolution. To distinguish between grid cells affected and not affected by sub-resolution changes of currents a threshold for the spectral power of the accuracy parameter is selected. All values below this threshold are assumed not to be affected by sub-resolution current changes (Figure 9 left hand side).

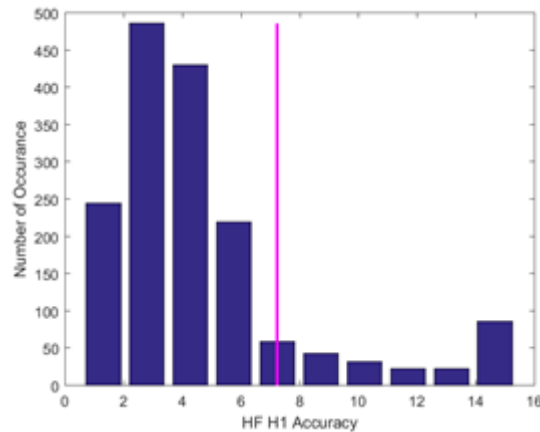


Figure 8: Histogram of the First Harmonic (H1) of the HF Accuracy. The vertical line (threshold value) separates the main distribution from the tail.

Figure 9 (left hand side) present a classification map, indicating the influence of the current-bottom interaction based on the scheme outlined previously. Figure 9 (right hand side) shows the classification map based on the same scheme but using the current modulation factor as an indicator. 87.1% of the grid points have the same classification label, i.e. influenced or not influenced by the bottom topography in both maps. Using the model results instead of HF-radar data the concurrence is 87.6%. If instead of the first harmonic the sum of fundamental mode plus first harmonic spectral power is used the concurrence is 85.9% for HF and 90.3% for model data.

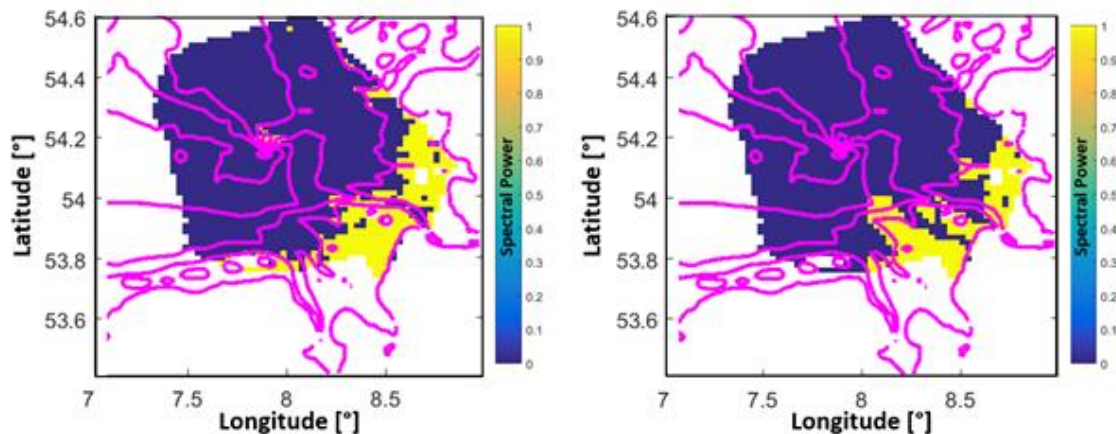


Figure 9: Classification of the area of coverage of the HF-radar station Büsum according to the expected influence of the bottom topography on subscale variations of the near-surface current.

This classification scheme is well suited to identify the influence of bottom-current interaction independently from technically ‘bad’ data due to technical problems, such as radar frequency interferences or the influence of 50 Hz noise from the electrical power supply.



### 3.1.2 Final assessment of common protocols and QC for HF radar data (CNR-ISMAR lead)

The work on common protocols for HFR data, metadata and QC in JERICO-NEXT has been carried on in strict collaboration and synergy with many ongoing initiatives coordinated by the EuroGOOS HFR Task Team, aiming at promoting the HFR technology in Europe.

Within JERICO-NEXT, work has been performed in several WPs, with WP2 devoted to harmonization, WP3 to research and WP5 to assembling recommendation for the common protocols. The first recommendation for a European Common data and metadata model for NRT HFR currents has been provided within the deliverable D5.13. Further research investigations aimed at modifying and improving the mandatory QC tests have been carried out in Task 3.2, while data format and data and metadata schemes have been found robust thus not requiring, at least at this stage, structural modifications. These investigations and finding have been reported in D3.3. All the discussions and activities have been carried on in strict collaboration with and with the support of the US colleagues managing the US Integrated Ocean Observing System (IOOS) through the Radiowave Operators Working Group (US ROWG). Also other important external contributions have been given by other networks, such as the Australian ACORN network.

In D3.4, the transition of the investigated improvements toward effective recommendations is reported. This has been done through the implementation of the proposed improvements within the final release of the European common data, metadata and QC model for NRT HFR current data, that has been recently published in the deliverable D5.14. Task 3.2 acted as the pivotal framework for improving protocols and boosting the network of the European HFR operators, building the foundations of the standardization process for ensuring data availability in standard formats.

The purpose of the format specification is to ensure both efficient and automated HFR data discovery and interoperability, with tools and services across distributed and heterogeneous earth science data systems. The European Common data, metadata and QC model for real-time HFR data is intended to be the unique model for HFR data distribution in Europe, thus it integrates CMEMS and SeaDataCloud (SDC) requirements. It complies with CF-1.6, OceanSITES, CMEMS IN-SITU TAC conventions (Copernicus-InSituTAC-SRD-1.4, CopernicusInSituTAC-ParametersList-3.1.0), and with the INSPIRE directive and the SDC CF extension requirements.

The data model also integrates the SDC requirements about the SeaDataNet metadata services (<https://www.seadatanet.org/Metadata>) for enforcing discovery and access of HFR data and in order to gain visibility and valorization for the projects and the institutions producing HFR data.





## 3.2 HF radar network developments (Subtask 3.2.2, Leader AZTI)

This subtask aims at providing a methodological guideline to design an integrated radar network at regional scale combining societal needs and HF radar properties. Up to now, the development of the HF radar networks in Europe has been locally driven by Maritime safety, Metocean monitoring and forecast, or Research (Mader et al., 2016; Rubio et al., 2017). The implementation of the in-situ component of the observing system is nowadays a responsibility of the member states. However, a clear trend is emerging revealing a need for European coordination in developing the Ocean Observing System (EOOS Strategy 2018-2022) and key initiatives like the Copernicus Marine Service, in collaboration with EuroGOOS, recently expressed requirements for the development of the in situ component in the different European regional seas (CMEMS requirements for the evolution of the Copernicus in-situ Component, Nov 2018, Mercator Ocean). The JERICO-Next Research Infrastructure Project has put in place the room for contributing as a coastal community in structuring homogenized networks for the key coastal platforms in Europe. In this task, we look for a way to share a joint strategy for developing the network with priorities to fill the existing gaps. This strategy is based on common drivers, targeted stakeholders and structures at European level, and regional considerations (more than national or local).

In the following pilot demonstration, the link between the societal needs and the role of the HF radar network will be illustrated. Then, a methodology to consider the impact of the HF radars operating frequency and site locations will be applied. These different steps will provide an assessment of different scenarios of installation for a HF radar network. The pilot area (IBI) includes Bay of Biscay and north-western Iberian Peninsula where transnational developments between France, Spain and Portugal would highly contribute to the existing national efforts. Finally, some numerical tools for integrating also information of the distributions and variability of ocean processes will be applied.

### 3.2.1 From the societal needs (AZTI)

The combination of networks of land-based HF radars could in principle provide a quasi-total coverage of the coastal area (as for instance along some regions of the US coast). However, mainly due to economic reasons, in practice only a limited number of systems can be considered along the European coast, and a need for prioritization of the network development arises. In order to address this problem, our first step aims at mapping the geographical distribution of the needs at regional level.

In this study, the map of observed vessel density has been used. to characterize spatially the requirements more directly linked with the application of HF radar data and products. This information has been chosen as a good proxy of integrated activities in the coastal area including Search and Rescue needs, possible sources of contamination (oil or chemical spills), fishing areas or ports areas. Recently, a EU Vessel density map has been made available by EMODnet Human activities portal (cf. EU Vessel density map Detailed method. V1.5 March



2019). This map has been made from ship reporting data of the Automatic Identification System (AIS), collected by coastal stations and satellites. It provides the total ship presence time on a 1 km grid, with monthly information and separately for 14 different ship categories (fishing, service, dredging or underwater operations, sailing, pleasure craft, high-speed craft, tug and towing, passenger, cargo, tanker, military and law enforcement). With QGIS software, the downloaded geotiff files have been converted to Geographical coordinates WGS84, then processed using Matlab ®.

The data available and used in this study are from the all Year 2017. In Figure 10, the total density with all ship categories is represented. The distribution of vessel density shows higher values in a longshore coastal area between the shoreline and around 50km, and weaker values in the offshore zone, except when a traffic separation scheme (or 'TSS') regulates the navigation of ships with intense lanes where the maritime traffic is concentrated. Moreover, the intensity in the coastal band is not homogeneous. Hotspots are identified mainly around fishing areas, the main ports and main maritime lanes, while gaps appear, for example in the middle of the Northern Spanish coast.

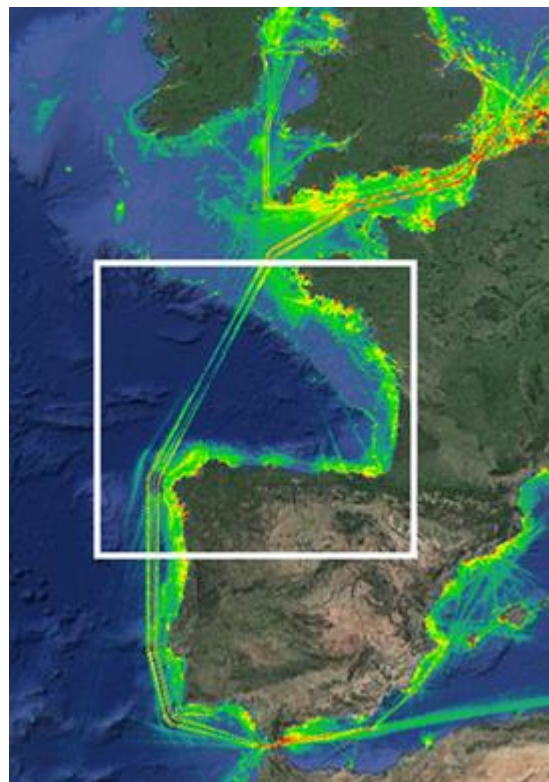


Figure 10: EU Vessel density map provided by <http://www.emodnet-humanactivities.eu/> (all vessel categories, Year 2017) and study area (white square)

### 3.2.2 Impact of the operating frequency on site location (AZTI)

The second step aims at mapping the theoretical characteristics of different scenarios of extended HF radar networks taking into account the operating frequency of the systems and the site locations. Common maximum coverage





for various direction finding systems operating respectively at 5 MHz or 13MHz are 180 km x 180 km and 70 km x 70 km, as given in Rubio et al. (2017). Upon deciding the use of specific frequencies, the wave climate must be considered. The Resonant Bragg Scattering, basic principle of the HF radars, depends on the wavelengths of the transmitted signal and surface waves. The needed ocean wavelengths for the two aforementioned frequencies are respectively around 30 m and 10 m. It represents a clear limitation for using long ranges (4-5 MHz) in closed basins like the Mediterranean or the Baltic seas. Other factors influencing the maximum range for surface current are the emitted power or the salinity. For low salinity (17-18) the range can be reduced between 25-40%, so this has to be taken into account when planning new radars in low salinity environments. In this study performed in the European Atlantic coast, the development scenarios only considered the use of Long Range systems (around 5 MHz) with average salinity of 35 psu and theoretical ranges of ~175 km. Note that these are theoretical ranges that could be limited by the aforementioned factors and also due to need for coordination of the use of the radio frequency bands between Administrations. The International Telecommunications Union (ITU) has advised that the separation distances between an oceanographic radar and the border of other countries shall be greater than 80-170 km over land, 200 – 920 km over sea depending on frequency and noise levels, unless prior explicit agreements from affected administrations are obtained. This could impose deployment limitations in many parts of the European coasts.

Moreover, to obtain surface current vectors, a HF radar installation must include at least two radar sites, each one measuring the radial velocity in its radial direction. Thus, once the radial components of the surface currents are calculated, they can be combined in the overlapping area to provide a surface current vector map. In the combination from radials to totals, the geometrical constraints regarding the angle between radials need to be taken into account. The Geometric Dilution Of Precision (GDOP, Chapman et al., 1997) is at the origin of systematic low reliability of velocity vectors at the edge of the observed domain, as well as along the baseline connecting receiving antennas. When considering possible locations of the radar sites, the geometrical constraints induced by the shape of the coastline will impact the expected GDOP error of the data.

In order to combine the requirement of maximum coverage and the technical limits of a Long Range (LR) HF Radar network in the pilot IBI area, a tool for GDOP mapping has been developed in Matlab®, based on the HFR\_Progs Matlab® package (<https://cencalarchive.org/~cocmpmb/COCMPwiki/>). The tool allows to compute maps of theoretical GDOP errors from a set of simulated radial grids from HF radar LR antennas. Figure 11 shows the application of the tool to the existing antennas along the IBI coast (from the EU HF radar inventory in Mader et al. 2017) and additional scenarios where several new antennas are added to the existing ones. Four scenarios have been considered: existing stations (Figure 11a), existing stations plus identified locations for future stations that could complete the existing systems (Figure 11b and 11c), maximum coverage scenario with existing antennas plus 12 new sites covering almost



whole the study area (Figure 11d). No detailed design study has been performed in this first approach. Typically, as previously described in other areas (Flores-Vidal et al 2015), the main geometrical effects are in the precision of the longshore component of the total current at the edge of the domain, and in the cross-shore component in some specific areas close to the coast due to baseline effect.

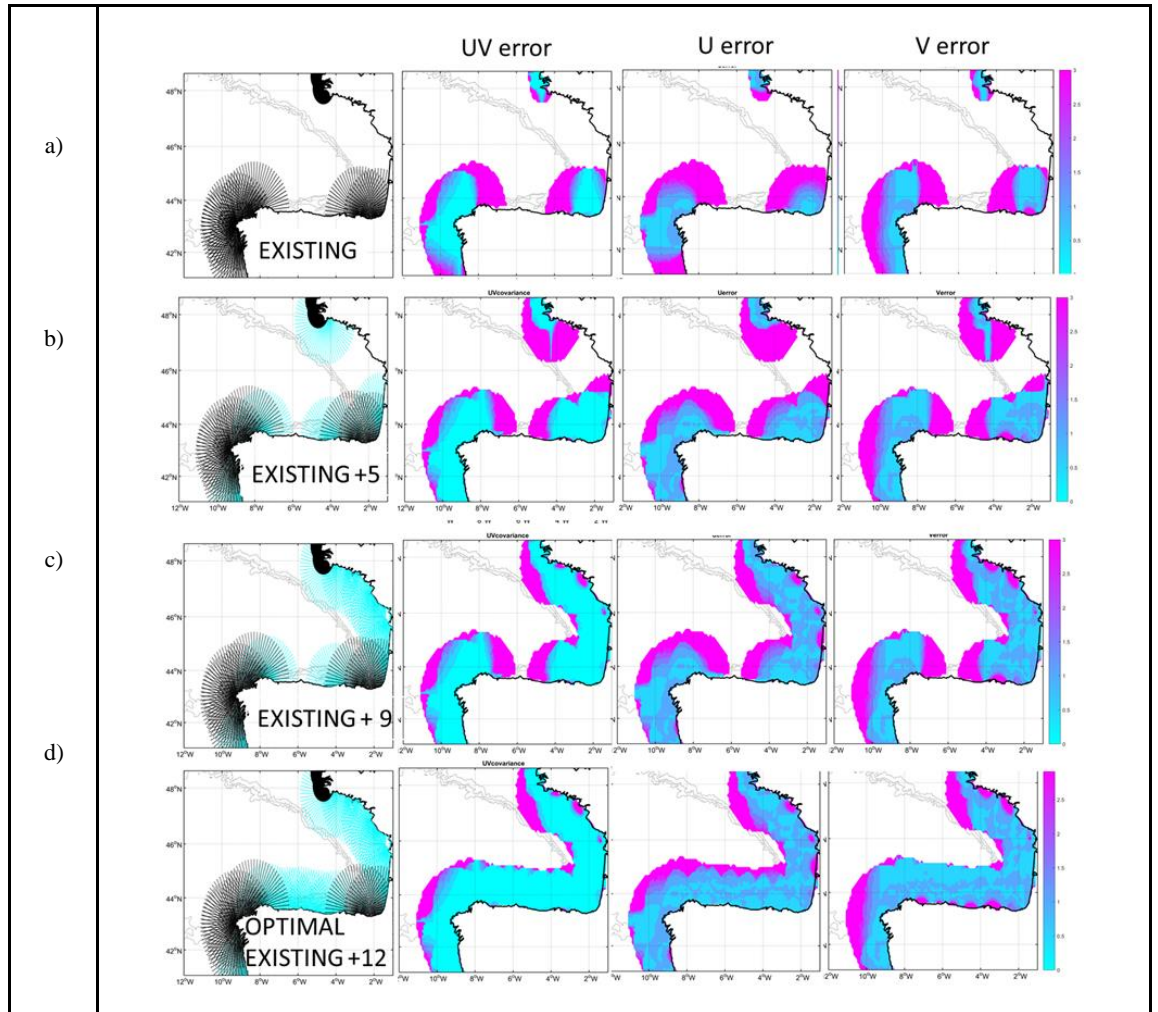


Figure 11: Different scenarios and associated GDOP errors (total, U and V components) for the pilot area in IBI based on the installation of a progressive number of HF radar Long Range sites.

### 3.2.3 Scenarios of development (AZTI)

In order to assess the impact of different scenarios of development of the HF radar network, a further step is taken combining theoretical error maps with information directly linked with specific applications of HF Radar data and products, using the vessel density maps as proxy of areas of more intense activity. In Fig.12, with a specific scenario of development (complete coverage adding Long Range HF radar stations), a mask based on a given threshold for the GDOP errors has been used to represent the network capacity associated to a specific marine activity, in this case fisheries (Category 1 of the EMODnet Human activities product Vessel density).

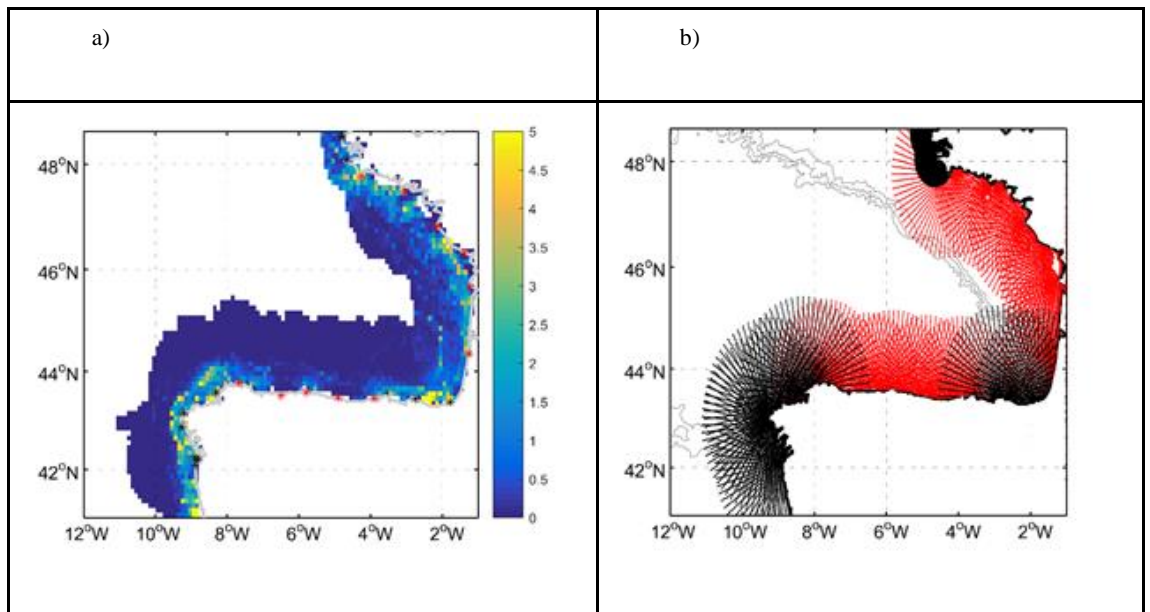


Figure 12: (a) Fishing vessel density map in the area of low GDOP errors for a scenario with complete HF radar coverage in the Bay of Biscay. The detail of radial grids is given in (b), where the (existing) new sites are plotted in (black) red.

Even if the requirements could be specified for the different marine activities with different weights depending on regional priorities, in the following analysis, we use the total of the vessel density, including all categories. In Figure 13, first, the two extreme scenarios have been mapped: (a) total coverage adding 12 Long Range stations; (d) existing coverage considering the 10 currently operated stations. Then, two intermediate scenarios have been defined: (b) removing 3 stations from the total coverage scenario in the middle of the Northern Spanish coast, where the requirement index is lower; (c) adding 5 adjacent stations to the existing network.

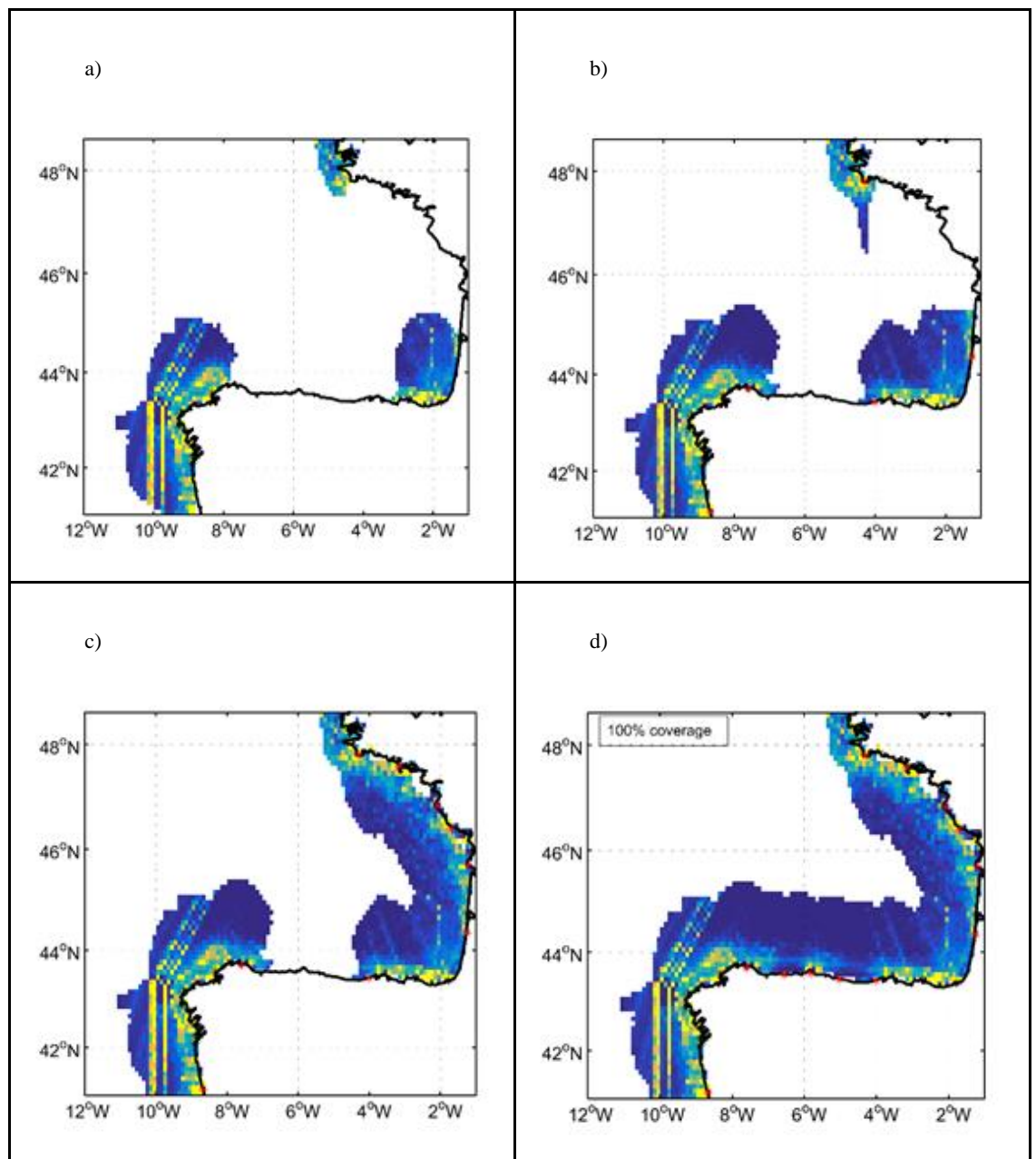


Figure 13: Total vessel density maps masked by different scenarios of HF Radar network; existing stations marked with black dots and new stations with red dots; (a) current network installed in 2019; (b) scenario adding 5 new stations to complete the existing systems (c) scenario adding 4 additional stations to better cover the French shelf where the requirement index is higher (higher vessel density); and (d) total coverage scenario.

In order to assess the respective contribution of the different scenarios taking into account the number of stations installed, the percentage of total covered area and vessel density for each scenario has been computed with respect to the total coverage scenario (Figure 14). We can observe that the benefits of expanding the existing network not only depends on the total number of new antennas added but mostly on their location. So the biggest gain is obtained with the installation of 5 new systems to complete the existing ones with a coverage 20% higher and 32% more vessels captured. The third scenario covering the French

shelf (4 additional new antennas) improves by approximately 20% both the coverage and density of vessels indicator with respect to the previous one. Finally, the addition of three new antennas over the Spanish coast in the total coverage scenario has a lower impact on the coverage (15%) and even less on the vessel density (4%), since it covers an area of low vessel traffic.

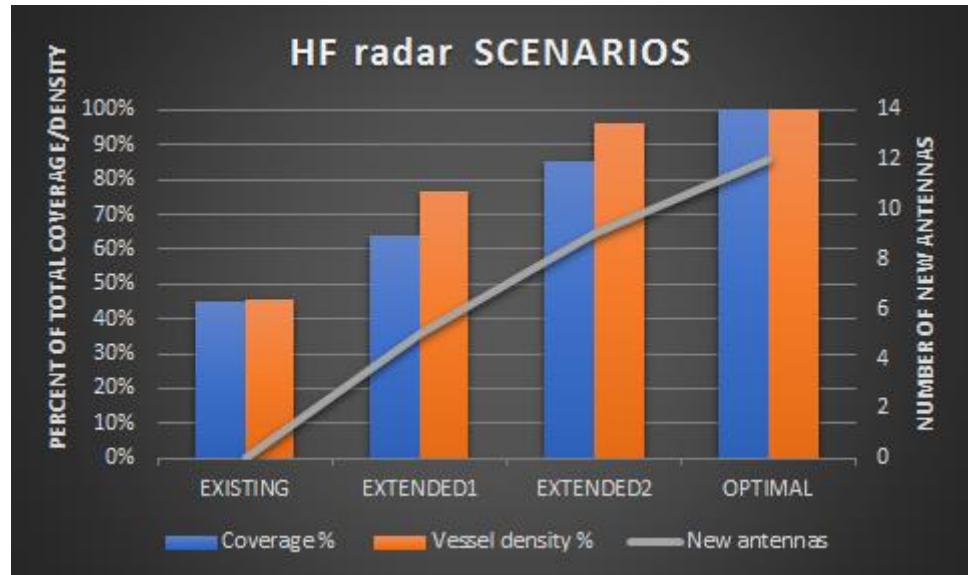


Figure 14: Scenarios assessment with respect to the total coverage scenario.

The main objective of this exercise was to show the potential of the developed methodology for planning the development of future networks. Further work can be done to improve the present tool by including additional information to build the scenarios (like different operation frequency) and the indicators in addition to the vessel density (like MPAs, or other vulnerability indicators).

### 3.2.4 Use of numerical tools for integrating the ocean phenomena distributions (IFREMER, CNRS)

In Task 3.7 of WP3 (Milestone 41 report), based on OSE/OSSEs methods, a first analysis has been implemented in the Bay of Biscay for designing a new radar site that will complete two existing stations (G. Charria, P. De Mey, Milestone 41 report and D3.11 Optimal OSE/OSSE infrastructure). Array Modes (ArM, Le Hénaff et al., 2009; Charria et al., 2016; Lamouroux et al. 2016) method, based on ocean model ensembles, has been used (Figure 15). The performances of two existing Bay of Biscay HF radar observation sites deployed on the Spanish Basque coast as well as a projected third site on the French Landes coast were evaluated (Figure 16). We characterized and visualized the model error structures which are detectable by the observations and which are potentially controllable through data assimilation. We showed that adding radars improves the detection of model errors by increasing the quantity and location of observations that lead to efficient sampling of model error structures. In particular, the third projected radar site would bring additional details at sampling zonal surface velocity errors in the model, because of its location.

Additionally, we studied the impact of correlated measurement errors on the ArM analysis. We found that our previous conclusions regarding the existing array performance and the positive impact of a third site were not significantly modified by such correlated noise contamination.

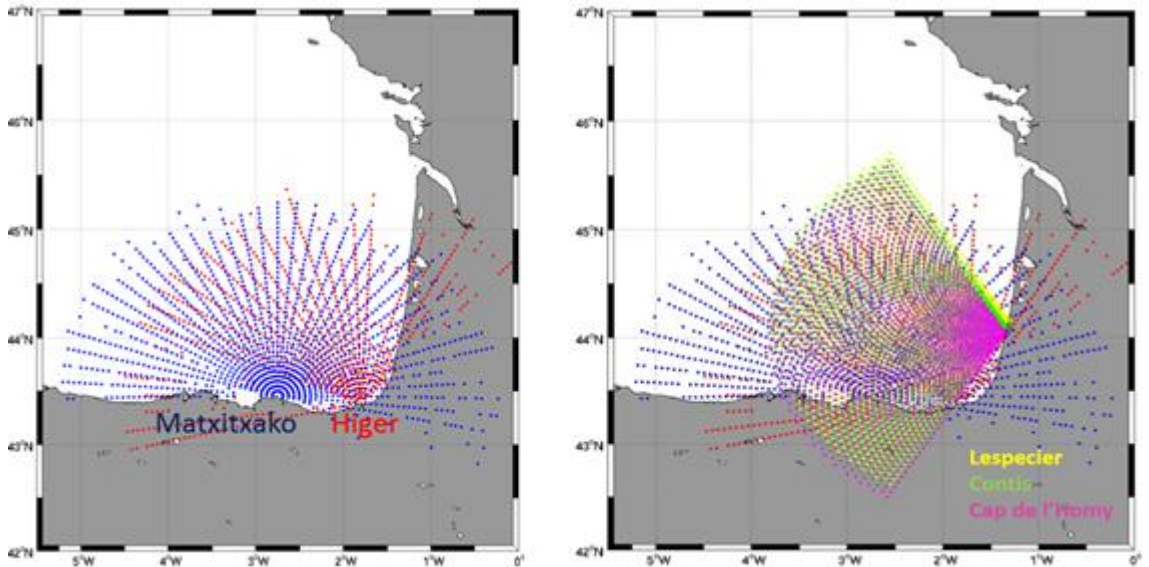


Figure 15: Illustration of three HF radar systems in the South-Eastern part of the Bay of Biscay including two existing systems (Matxitxako and Higer - left) and a future system to be deployed during JERICO-NEXT in 2019 (called "Lespecier" - right).

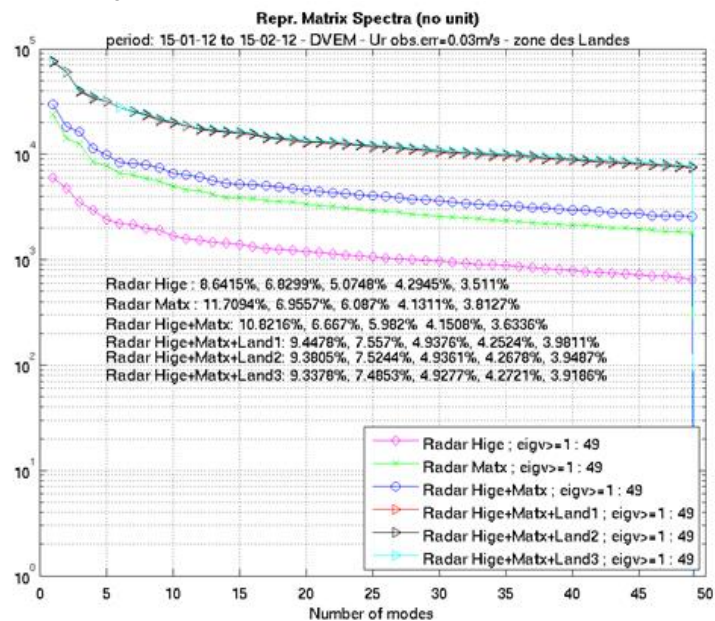


Figure 16: Repr. Matrix Spectra with and without the new HF Radar for three potential deployment sites (Land1, Land2, Land3). Adding radars improves the detection of model errors (shown in plot as eigenvalues ~7 times bigger) by increasing the quantity and location of observations that lead to efficient sampling of model error structures.

The user-friendly open-source tool, called Stochastic ocean Observing Network Assessment Toolkit (SONAT), developed by Actimar for IFREMER and CNRS, allows to extend the application of this methodology for assessing multivariate, multiplatform ocean observation networks. It will provide an opportunity to





integrate a quantitative characterization of the distribution of ocean phenomena in the analysis, highlighting the key role of observing network in monitoring ocean variability. It will also provide a direct assessment of the impact of the different scenarios of development of the network for improving the performance of data assimilation modelling configurations.

### **3.3 New products for 4d characterization of shelf/slope hydrodynamics and transport (Subtask 3.2.3, Leader CNR-ISMAR)**

In this subsection, results from Subtask 3.2.3 are reported in terms of development of new methodologies that can be used as tools for HF radar data analysis and practical applications. Results from Subtask 3.2.3 were not included in D3.3, and they are all included in the present D3.4. A number of new results have been obtained and they have been first tested in a methodological way and then applied to HFR data sets in specific sites, in some cases in synergy with WP4 JRAPs. In the following we introduce the new methods and illustrate their testing and assessments.

#### **3.3.1 Merging HF radar and water column data (CNR-ISMAR, AZTI)**

One of the main aims of the sub-task is to provide methods that allow to combine surface velocity information from HFR with water column information from other instruments such as gliders or ADCPs, in order to contribute to the assessment of 3 dimensional (3d) transport and its impact on the distribution of pollutants and biological quantities.

We concentrated mostly on coastal boundary currents, that are especially relevant to the Jerico multiplatform system. Boundary current velocity has various components, including mesoscale geostrophic velocity, and ageostrophic sub-mesoscale velocities including wind driven response. These components strongly differ in scales. In particular, mesoscale flows typically extend in the vertical until the main thermocline (order of more than 100 m), while wind driven flows are typically restricted to the upper mixed or Ekman layer (order of 10-50 m). It can then be expected that HFR surface velocity (order of 1m from the surface) is a combination of geostrophic and ageostrophic components, while deeper information from ADCPs are mostly influenced by the geostrophic currents. In the case of gliders, only geostrophic velocities are known, since gliders provide hydrographic profiles (temperature T and salinity S) from which geostrophic velocities are estimated.

##### **3.3.1.1 Separating geostrophic and wind driven velocity using HFR and glider data (CNR-ISMAR)**

An important first step for combining HFR and water column data is to unravel the various components of the surface velocity. At this end, a method has been developed using jointly HFR and glider data (Berta et al., 2018). The glider data are used to estimate geostrophic velocity along the water column, and they are compared to the total HFR velocity at the surface. The difference between the two provides an estimate of the ageostrophic component, that in general is due



to wind driven and sub-mesoscale instabilities. In the case of a well developed strong boundary currents it can be assumed that geostrophic and wind driven velocities are the two main components, so that they can be effectively separated. The method has been tested using HFR and glider data in the Northern Current (NC) in front of Toulon (Figure 17), considering a period of 2 weeks in December, when strong wind events occur.

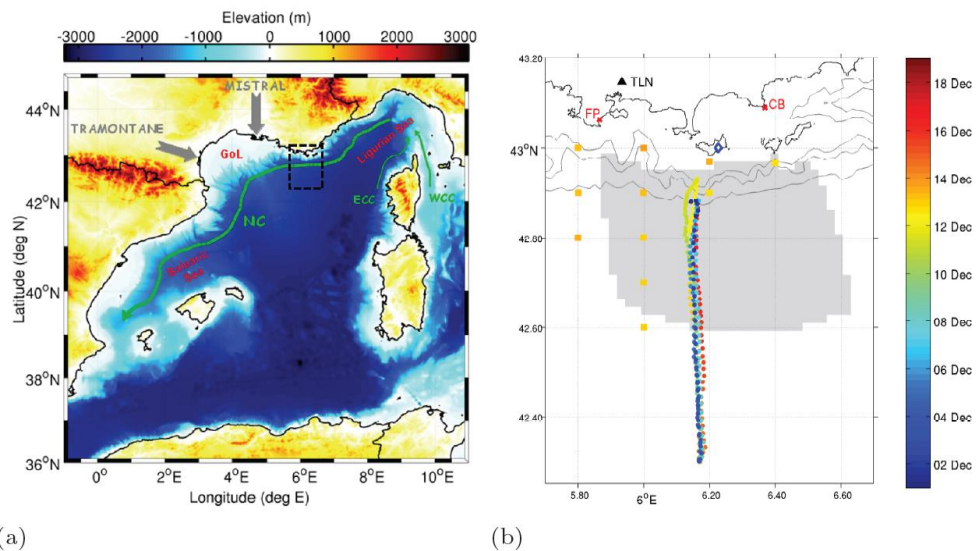


Figure 17: (a) The Western Mediterranean Sea, including northern circulation branches and main winds. The region of study is marked as a dashed black square. The following acronyms are used: GoL: Gulf of Lion, NC: Northern Current, WCC: Western Corsica Current, ECC: Eastern Corsica Current. (b) Details of the region of study including the synoptic measurements carried out during the experiment (December 2-19). The gray area is the HF radar surface current field coverage, while the two red crosses indicate the HF radar sites at Fort Peyras (FP) and Cap Benat (CB), in the Toulon (TLN) area. The orange squared marks represent the CTD stations, while the dots array at 6.20° E is the track of the repeated glider transects. CTD stations and glider tracks are color coded in time. The blue diamond indicates Porquerolles wind station's position. Bathymetric lines at 500 m, 1000 m and 2000 m depth.

When the wind is weak, the current is found to be mostly zonal and in geostrophic balance even at the surface, with an associated zonal transport of 1 Sv Figure 18 a). During strong upwelling-prone westerly wind events (longer than 2–3 days) an interplay between the direct-wind-induced ageostrophic response and the geostrophic component is observed, with offshore surface transport, surface cooling, flattening of the isopycnals, and reduced zonal geostrophic transport (0.5–0.7 Sv). The sea surface response to wind events, as observed by the HF radar, shows total currents rotated at about 55° to 90° to the right of the wind (Figure 18 b, c). Performing the decomposition between geostrophic and ageostrophic components of the surface currents, the wind-driven ageostrophic component is isolated and is found to rotate by about 25° to 30° to the right of the wind (Figure 18 d). The ageostrophic component magnitude corresponds to 2% of the wind speed.

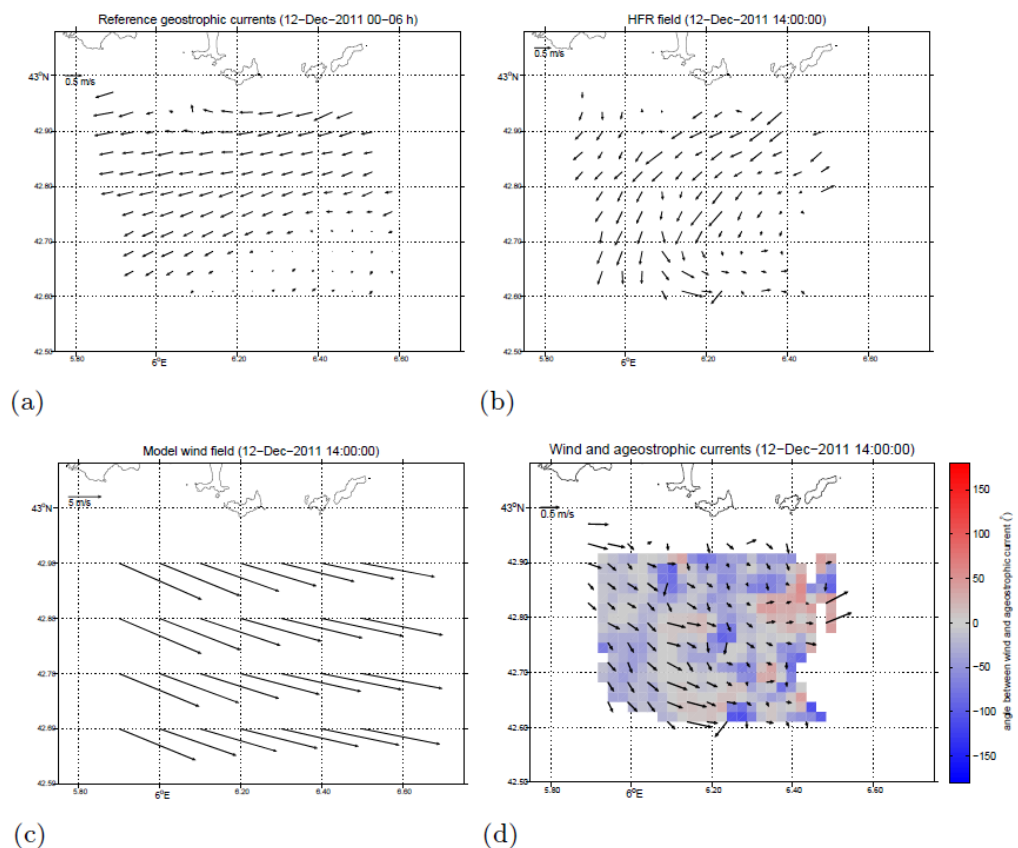


Figure 18: Example maps of: (a) 6h time-averaged geostrophic flow derived from HFR prior to the wind onset, (b) instantaneous HFR surface currents during the wind event, (c) ALADIN wind field, and (d) ageostrophic surface currents superimposed on the color coded map quantifying the angle between the ageostrophic component and ALADIN wind. Negative values means current to the right of the wind.

### 3.3.1.2 Toward blending HF radar and ADCP velocities (AZTI, CNR-ISMAR, JTC, IEO)

Velocity data from surface HF radar and ADCP water column have been blended using and testing two different blending methods. The combination of the data obtained from multiplatform observing systems is an interesting approach for a better understanding of the three-dimensional coastal circulation. The application of data-blending methods to observations with complementary spatial coverage can be used for extending the information to the nearby areas or vertically through the water column. In the case of HF Radar, the combination with observations in the water column is especially interesting since it can broaden the application of the data to biological, geochemical and environmental issues, since plankton or pollutants can be located deeper in the water column and not only follow surface dynamics.

Here the skills of two data blending methods applied to current velocity are investigated and tested in the SE-BoB area: the DCT-PLS method proposed by Fredj et al. (2016) and the ROOI method proposed by Jordà et al. (2016). The former is based on a penalized least square (PLS) regression approach combined with a discrete cosine transform (DCT) method, and is based on a purely statistical approximation. The latter is based on a reduced order optimal

interpolation (ROOI) fed with spatial covariance matrix, which adds prior physical information to the method. The main characteristics of the methods are schematized in Tab 1,2.

<b>Discrete Cosine Transform Penalized Least Square (DCT-PLS)</b> (García, 2010; Fredj et al., 2016)
✓ Gap-filling method based on penalized least squares regression
✓ The fitting model based on DCTs and a smoothing (fitting) parameter $s$ .
✓ Test the fitting for each $s \rightarrow$ by cross validation $\rightarrow$ GCV score <ul style="list-style-type: none"><li>➢ GCV score estimated by the expected trade-off (F) between:<ul style="list-style-type: none"><li>• the bias of the fitting (RSS)</li><li>• the variance of the results of the created model (P).</li></ul></li></ul>
$F(s) = \text{RSS} + \text{P} = \ y - \hat{y}\ ^2 + s\ D\hat{y}\ ^2$ $E[F] \rightarrow \text{GCV}$
✓ The best fitting model is obtained from the minimization of the GCV score. $\min(\text{GCV}) \rightarrow s$

Table 1 Main characteristics of the DCT-PLS method. GCV: Generalized Cross Validation, see Fredj, 2016 for further details.

<b>Reduced Order Optimal Interpolation (ROOI)</b> (Kaplan et al., 2000; Jordà et al., 2016)	
✓	Reduced Order Optimal Interpolation (Kaplan et al., 2000)
✓	Fed with historical data by means of a spatial covariance matrix
✓	The reconstructed field (Z) is obtained by means of: <ul style="list-style-type: none"><li>➤ the spatial EOFs (U) of the covariance matrix</li><li>➤ the corresponding set of amplitudes (<math>\alpha = U^T Z</math>)</li></ul> $Z = U \cdot \alpha$
✓	Only the leading M modes that explain a high percentage of variance are considered (reducing the order). $Z_M = U_M \cdot \alpha_M$
✓	The amplitude ( $\alpha_M$ ) is obtained from the minimization of a cost function that accounts for: <ul style="list-style-type: none"><li>➤ the difference with the available observations</li><li>➤ the observational error</li><li>➤ not giving too much energy to higher order modes</li></ul>

Table 2 .Main characteristics of the ROOI method

To test the skills of methods, they have been applied to pseudo-observations of currents extracted from the IBI CMEMS model field (ATLANTIC-IBERIAN BISCAY IRISH- OCEAN PHYSICS REANALYSIS), simulating a real observatory configuration in the area. The outputs of the methods are compared with the IBI model data, which is also used as the synthetic 'truth'. The observations considered are: a) surface current field (simulating HF radar measurements) and b) current velocity profiles at two locations over the slope (simulating data from two ADCPs collocated on two slope buoys) (Fig.19)

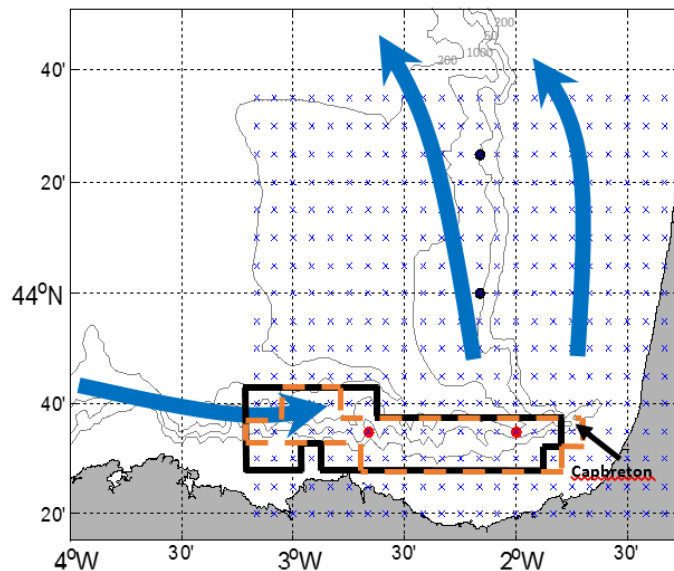


Figure 19. Main characteristics of the study area. The winter typical circulation is represented by blue solid arrows). The grid used for the simulated HFR surface current fields is shown by blue crosses. The red dots provide the location of the current vertical profiles in the location of EuskOOS buoys: Matxitxako (left) and Donostia (right), whereas the black dots depict the location of the two extra buoys used for the 4-buoy scenario. The bold black lines delimit the winter reduced grid, whereas the intermittent orange lines delimit the summer one.

For the DCT-PLS method, the only inputs are the pseudo-observations obtained from the IBI CMEMS model. For the ROOI method, also the covariance matrix has to be provided. For this last case, different historical datasets have been used to infer the spatial covariances (in order to be able to assess the performance of the method with more and less realistic cases). The following cases have been considered: the IBI model data itself, as the ideal blending case where the covariances are completely consistent with the pseudo-observations; a high resolution (HR) reanalysis product (GLOBAL OCEAN PHYSICS REANALYSIS GLORYS12V1), which provides similar results to IBI (but independent); and a low resolution (LR) reanalysis product (GLOBAL OCEAN PHYSICS REANALYSIS GLORYS2V4) that offers the most realistic and challenging scenario since the obtained covariances are completely independent of the pseudo-observations (obtained from IBI CMEMS model) and the low resolution of the model grid is not resolving properly the mesoscale contained in the pseudo-observations.

First results were obtained for winter 2011, when the circulation is mainly driven by the slope current in eastward direction along the Spanish slope and northward along the French slope. Results are presented in terms of RMSDs between the outputs of the methods and the IBI 'truth' data. If we consider the LR reanalysis product, which is, as mentioned, the one that provides the most realistic case, it is shown that the ROOI method provides the best results for the U component if we consider the whole study area. Similar results using both methods are obtained for V and in general in the areas with high density of observations (Figure 20).

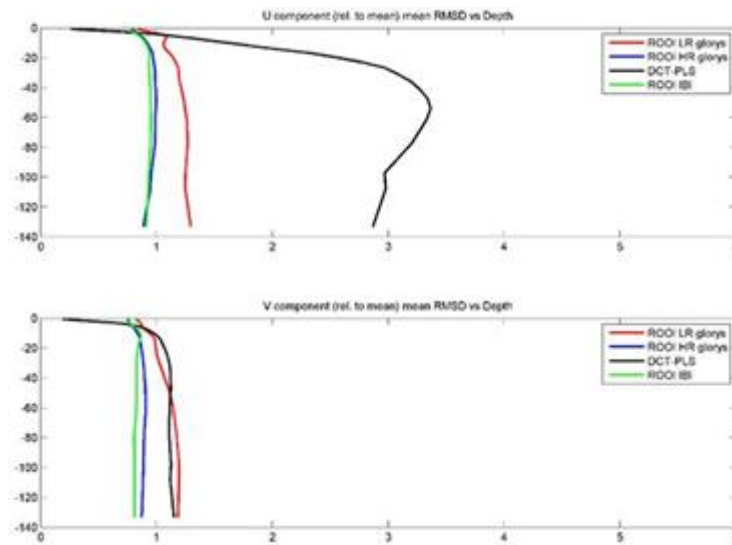


Figure 20 Mean RMSD relative to the mean current (of each grid point) for each depth (in meters). For component U (top) and component V (bottom). The results obtained using DCT-PLS and ROOI (using different datasets for the covariance matrices) are shown.

To further explore the performances of the two methods, we have plotted the spatial distribution of the relative RMSD for the U component between the reconstructed and reference fields (Figure 21). For the ROOI method we can observe that the relative RMSDU shows globally lower values when considering the whole study area, while the performances DCT-PLS method, the RMSDs are lower near the areas of high density of observations, and higher out of those areas.

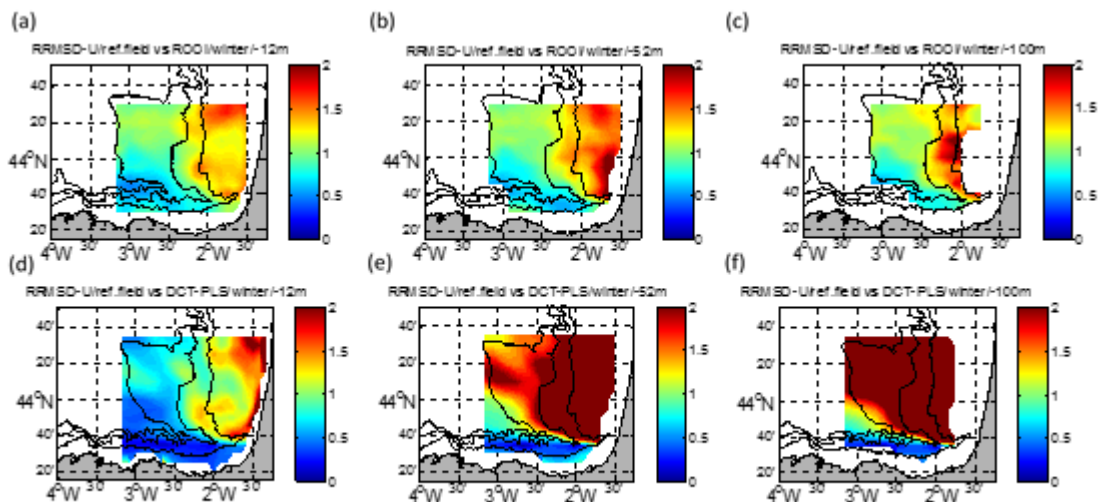


Figure 21. Maps of RMSD relative to the mean current (at each grid point) for each depth (in meters) between the reference fields and the outputs of the ROOI (a-b-c) and the DCT-PLS (d-e-f) method, for the U component and winter.

The results of the comparison of the DCT-PLS and the ROOI methods indicate that each method has its pros and cons. The DCT-PLS method only needs data



from observations, it does not need any extra information about the study area. However, the absence of that extra information also makes the reconstruction less robust and therefore provides worse results out of the areas of high density of observations. On the other hand, the ROOI is a robust data-reconstruction method that uses historical information of the study area, providing better results than the DCT-PLS method in areas far from the observations. Nevertheless, this method needs prior historical information of the study area. Another weakness is that an appropriate initial parameter needs to be set; in a real scenario the outputs of the reconstruction could not be assessed in order to find the best parameter. Cross-validation methods could be used setting some gaps on the data, in order to find out the most appropriate value.

These data-reconstruction methods could provide a wide range of applications. For instance, they could be used to obtain new operational products, combining data from different sources and complementary spatial coverage, due to their low computational cost. These costs vary depending on the number of grid points considered and on the length of the historical data used for the ROOI method. These data-reconstruction methods also have a potential usefulness as testers in order to predict the improvement of the sampling for different coastal observatory scenarios, thus, providing a potential tool for making decisions for future planning of coastal observatories. Additionally, they might have applications for coastal risk assessment or for model validation as well.

As a next step, applications of the ROOI method are planned using real historical data from HF radar and ADCP buoys in the SE Bay of Biscay (SE-oB).

(This work is being prepared for submission to a peer review journal and has been presented in the EGU GA 2019 - Three-Dimensional Reconstruction of Ocean Current Circulation from Coastal Marine Observations: Challenges and Methods. Authors: Ivan Manso-Narvarte (AZTI), Erick Fredj (Jerusalem College of technology, Israel), Gabriel Jordà (IEO, Spain), Maristella Berta and Annalisa Griffa (CNR), Ainhoa Caballero and Anna Rubio (AZTI))

### **3.3.1.3 Toward blending HF radar and glider data (AZTI, CNR-ISMAR)**

The next step (in progress) is to apply the methods to the blending of HF radar data with glider data, first using synthetic data and then with real in-situ data.

An application of the method DCT-PLS is under way in the Northern Current, using outputs from the GLAZUR hydrodynamic model, following an OSSE approach.

Differently from the ADCP case, the glider depicts only the geostrophic component of the velocity and the previously introduced decomposition between geostrophic and wind driven velocity (Berta et al., 2018) is expected to play an important role. A preliminary test of the DCT-PLS method has been done and the results are encouraging (Fig,22).

Second, new data obtained in the BoB in the framework of the BB-Trans glider campaign will be used for a more complete data blending exercise. During the BB-Trans glider campaign, held in the period 17 May- 14 June 2018, a deep and a shallow-glider measured the water column in an area covered by the HF radar. The Slocum deep glider was equipped with a CTD, ADCP, fluorescence-turbidity and MicroRide sensors, and measured the water column from the surface to at a maximum depth of 1000 m. During the mission, besides the glider tracking that allowed to monitor the position and the data measured by the glider, surface current fields and derived Lagrangian Residual Currents (LRC) (Fig. 23, along with images from satellites, were used to change when necessary the next positions and setting of the glider in a near real time. In several instances, the glider tracks followed the tracks of the Sentinel 3A's 257 and Jason-3's 248. The analysis of the data from both gliders are in progress.

Overall, the new collected data set consists of glider data, HF radar data, Jason-3 (track 248) and Sentinel-3A (track 257) altimeter data (Fig.23), and Donostia buoy ADCP data. These measurements will allow to fully test different methodologies of data blending for deriving transport in the water column. In addition to this, they will also be used to evaluate the accuracy of coastal altimetry along-track data in the study area.

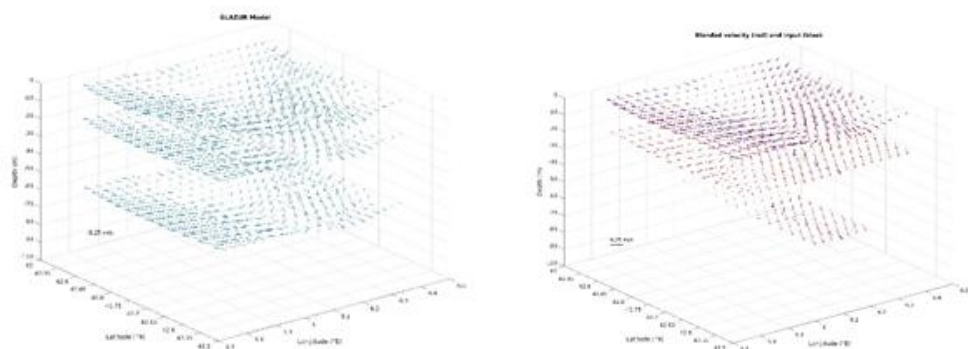


Figure. 22. In the left panel 3D currents from model output used as ground truth for testing the DCT-PLS blending method. In the right panel 3D current blending (red arrows) starting from selected model currents information (blue arrows) at the surface (representing HF radar data) and along a section (representing a glider transect).

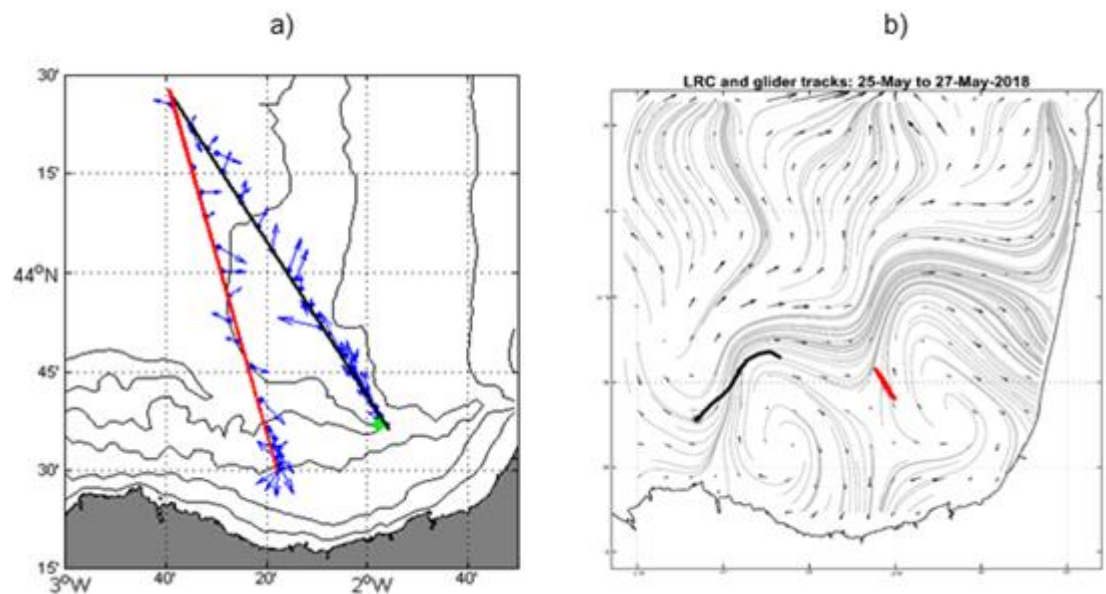


Figure 23. (a) Tracks of the two altimeters crossing the area during the mission (the black/red line represents the track of Jason 3/Sentinel 3A) and vertically integrated currents corresponding to the deep glider (blue arrows). (b) Lagrangian Residual Current maps estimated from the HFR data and corresponding to 25 to 27 May 2018 show well defined mesoscale structures in the area during the glider campaign. The trajectories followed by the deep-glider (red line) and shallow-glider (black line) during this period are also shown (the asterisks indicate the beginning of the trajectory).

### 3.3.2 Gap filling techniques (IMEDEA UIB-CSIC, SOCIB, AZTI, CNRS-MIO)

In the last years, the use of Lagrangian metrics to study mixing and transport properties has been growing in importance. A common condition among all the Lagrangian techniques is that complete spatial and temporal velocity data are required to compute trajectories of virtual particles in the flow. The increased availability of high-frequency continuous surface currents derived from HF radars, is providing new possibilities for the application of Lagrangian methods to these observations for understanding small-scale transport processes in the coastal ocean. However, hardware or software failures in the HFR systems can compromise the availability of data, resulting in incomplete spatial coverage fields or periods without data. In this regard, several methods have been used in the literature to fill spatiotemporal gaps of HFR measurements. Despite the growing relevance of these systems there are still many open questions concerning the reliability of gap-filling methods for the Lagrangian assessment of coastal ocean dynamics. Here, available gap-filling techniques such as open-boundary modal analysis (OMA) and data interpolating empirical orthogonal functions (DINEOFs) have been investigated, and a new methodology has been developed based on self-organizing maps (SOMs).

The OMA (Kaplan and Lekien, 2007) is based on a set of linearly independent modes that are calculated before they are fit to the data. These modes describe all possible current patterns inside a two-dimensional domain (taking into account the open boundaries and the coastline). The amplitude of those modes is then fitted to current measurements inside the domain. OMA considers the

kinematic constraints imposed on the velocity field by the coast since OMA modes are calculated taking into account the coastline by setting a zero normal flow. Depending on these constraints they can be limited in representing localized small-scale features as well as flow structures near open boundaries. Difficulties may arise when dealing with gappy data, especially when the horizontal gap size is larger than the minimal resolved length scale (Kaplan and Lekien, 2007) or when only data from one antenna are available. In the case of large gaps, unphysically fitted currents can be obtained if the size of the gap is larger than the smallest spatial scale of the modes, since the mode amplitudes are not sufficiently constrained by the data (Kaplan and Lekien, 2007). This is why when using OMA, it is recommended to reach a compromise between the number of modes used for spatial scales larger than the largest gap and a sufficient number of modes correctly representing the spatial variance of the original fields (knowing that the spatial smoothing increases as the number of modes decreases).

The case of data from a single antenna (CODAR system) or antenna net (WERA system), also known as the case of orphan HFSWR site, has been further investigated. It has been found that the OMA method can still be used under the conditions of robust radial velocity estimates and little horizontal gaps. This can be achieved when using radial velocities averaged on one inertial period, hence removing inertial variability and filling small spatial gaps, as shown in Fig. 24. Likewise, it has been found that using altimetry derived geostrophic currents to introduce some constraints in the far field may help to limit unrealistic small-scale flow structures near open boundaries.

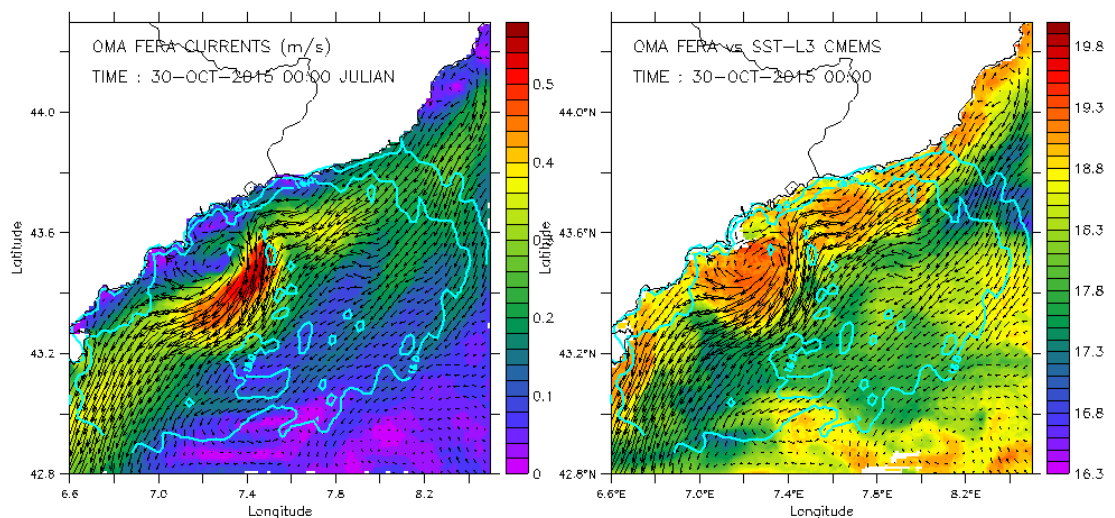


Figure 24: This is one example of the performance of OMA method in building the current field based on only one radial velocity component at the coast with one antenna based in Saint-Jean Cap Ferrat, and constrained by the geostrophic current deduced from the Absolute Dynamic Topography (Aviso/CMEMS) at more than 60 kms from the coast. The left panel shows the current field reconstructed by OMA and averaged on one inertial period (17 hours centered on 30 october 2015). The right panel shows the sea surface temperature and superimposed the same current field. The hot core seen on the SST at the south of the Var river (around Nice) and the associated frontal zone are coherent with the structure of the current field (eddy)



The DINEOF is an iterative methodology used to interpolate gaps or missing data in geophysical datasets (Beckers and Rixen, 2003; Alvera-Azcárate et al., 2005). The method was initially applied to sea surface temperature and ocean color (e.g., Alvera-Azcárate et al., 2005, 2015; Ganzedo et al., 2011; Volpe et al., 2012; Esnaola et al., 2012; Beckers et al., 2014), but the technique has also been used for other variables like sea surface salinity (Alvera-Azcárate et al., 2016) and surface currents from HF radar (Hernandez-Carrasco et al., 2018). The technique is applied to an  $N \times M$  data matrix, where  $N$  is the size of spatial locations of the geophysical field, and  $M$  the time dimension of the data. Before the methodology is initialized, part of the initially non-missing data is removed from the data matrix and stored for cross-validation. Then anomalies are computed by removing the time mean at each location, and gaps or missing data are replaced by zero-value anomalies. At this point the data matrix is iteratively decomposed and rebuilt by means of an EOF analysis with a fixed number of EOFs. Values of originally missing gaps evolve through this iteration until convergence is met. (Open source DINEOF Fortran code: <http://modb.oce.ulg.ac.be/mediawiki/index.php/DINEOF>)

Concerning the new methodology developed here (and recently published by Hernandez-Carrasco et al. 2018), it is based on the Self-organized Models (SOM). SOM is a powerful visualization technique based on a neural network of unsupervised learning, which is especially suitable for extracting patterns in large data sets (Kohonen, 1982, 1997). In this way, SOM is able to compress the information contained in a large amount of data in a single set of maps.

For the reconstruction of HF radar currents, the SOM technique is applied to the domain, using as an input vector the radial velocity maps at each time (so, each neuron corresponds to a spatial pattern of characteristic radial velocity over the coverage area of the HF radar). Since each time step has an associated time and location, the time of a given spatial pattern which is the observed field that best matches that pattern can be obtained, providing a time series of the corresponding spatial pattern. From this configuration, a simple algorithm for filling holes is constructed, consisting of the following steps: (i) Training process. The radial velocity maps of the HF radar are used as input to feed the neural network iteratively; (ii) Spatial patterns. Once the training process is finished, we obtain an ordered neural network of spatial patterns of radial velocities without gaps; (iii) Identification of the holes. The position and time of the points of the mesh containing data gaps are located; (iv) Filling gaps. The SOM spatial pattern most similar to the HF radar radial velocity map with gaps is identified and used to replace the missing values.

The performance of each approach is quantified in the Lagrangian frame through the computation of finite-size Lyapunov exponents, Lagrangian coherent structures and residence times. We determine the limit of applicability of each method regarding four experiments based on the typical temporal and spatial gap distributions observed in HFR systems unveiled by a K-means clustering analysis. Our results (Fig.25) show that even when a large number



of data are missing, the Lagrangian diagnoses still give an accurate description of oceanic transport properties.

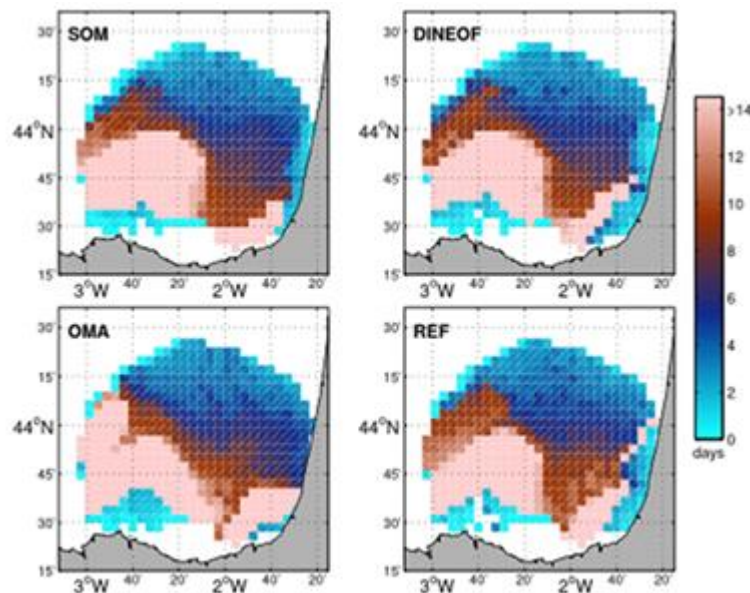


Figure 25. Snapshots (April 04, 2013 18:00) of Residence Times computed from the three filled and the reference HF Radar data for a scenario representing a decrease in bearing coverage in one of the antennas (more details in Hernandez-Carrasco et al, 2018).

### 3.3.3 Lagrangian techniques and products for biological and environmental applications (CNR-ISMAR, IMEDEA UIB-CSIC, SOCIB, AZT)

HF radars provide hourly maps of surface velocity that can be used to compute Lagrangian statistics and quantify transport and retention. This has consequences for the transport of pollutant, nutrients, larvae and eggs, and is therefore relevant to biological and environmental applications. Examples of methodologies and applications are provided below.

#### 3.3.3.1 Lagrangian techniques to quantify transport (IMEDEA UIB-CSIC, SOCIB, AZTI)

Once we have gap-filled data, we can use Lagrangian techniques to explore different transport processes. Two examples of applications of Lagrangian techniques have been performed in collaboration with the JRAP4 in the SE-BoB area regarding the study of the eddy-induced cross-shelf export of high Chl-a waters. For that end, different Lagrangian approaches were used on HFR velocities. For all of them, a 2D-version of the Lagrangian Particle-Tracking Model (LPTM) was implemented to simulate particle trajectories using HF radar velocities (see Rubio et al., 2018 for further detail). The LPTM solves the path of the particles with a fourth-order Runge–Kutta scheme permitting the computation of multiple trajectories with a low computational cost.



A comparison of virtual trajectories obtained from this model using HFR velocities and real trajectories from drifters deployed in the study area (Solabarrieta et al., 2016), demonstrates the skills of the LPTM applied to different HFR products (including OMA fields).

Then, LCS and FSLEs, escape rates and connectivity computations were obtained from specific processing of the resulting trajectories.

LCS can be computed from ridges in the FSLE field, which are arranged in filamental structures (d'Ovidio et al., 2004; Hernández-Carrasco et al., 2011). Here, the role of the eddy and frontal dynamics in organizing the coastal flow was analysed by means of the LCS derived from the hourly HFR velocities, following the works by Shadden et al., (2005), Haller and Yuan (2000), and Haller (2015). LCS are obtained computing the maximum values of the FSLE field that are located in a line-like shape (Joseph and Legras, 2002; d'Ovidio et al, 2004; Hernández-Carrasco et al, 2011).

FSLEs are the adaptation of the classical definition of the asymptotic Lyapunov exponents to finite time and spatial scales (Aurell et al 1997; Boffetta et al 2001). FSLEs from the HFR velocity fields were obtained at each instant, by computing the time  $T$  employed by pairs of particles, initially separated by a given distance, to reach a final distance. This Lagrangian approach assumes that any particle at the ocean surface is advected by the flow with a trajectory that can be recovered from the HFR velocity.

In our computations, we used an integration time step of 10 min with a bi-linear interpolation and a total period of integration of 30 days (in December 2014). Particles escaping the area before reaching the final separation were not considered in the analysis. Due to the small size of the HFR coverage area, the computation of the FSLE was calibrated, such that the FSLE provide robust and relevant LCS. Figure 26 shows the evolution of the FSLE field for the simulation period 10-20 December 2014.



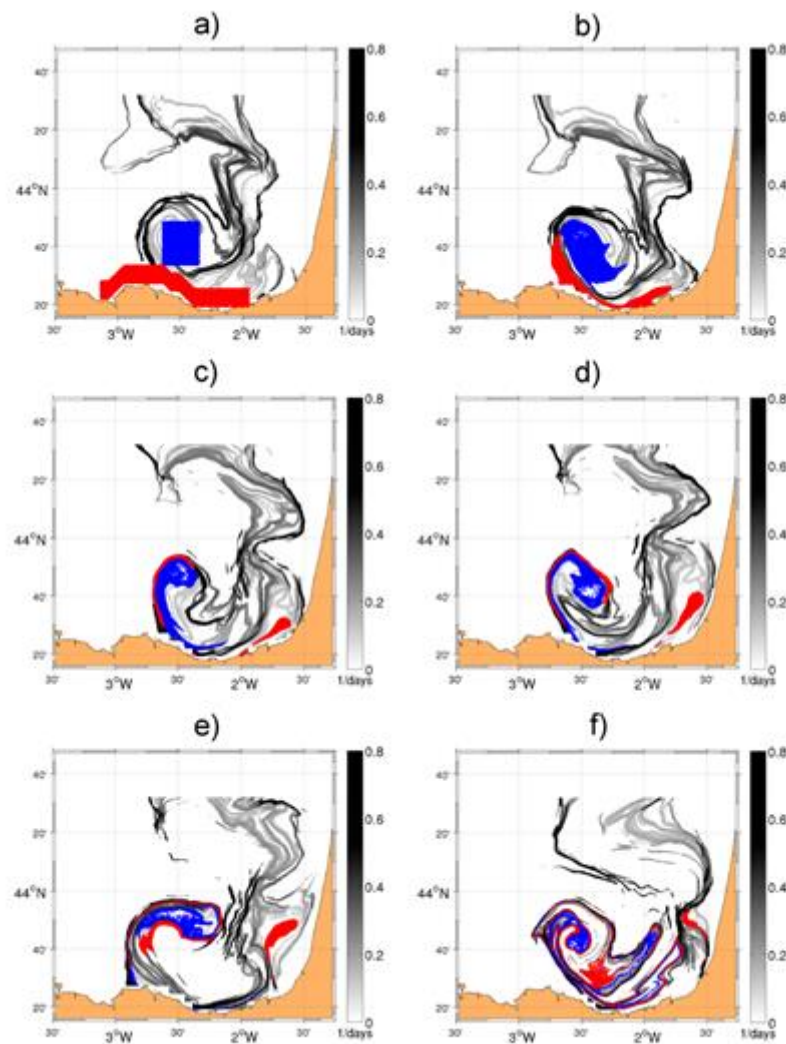


Figure 26. Evolution of the FSLE field (grey colorbar) for the simulation period 10-20 December 2014. Particles in red illustrate the evolution of shelf waters, while those in blue illustrate the behaviour of particles initially located within the eddy core. Dates and times of the snapshots are: (a) 10 December 12:00, (b) 11 December 16:00, (c) 13 December 08:00, (d) 14 December 08:00, (e) 16 December 08:00, (f) 20 December 08:00.

Using the results, we studied the characteristic time-scales for transport processes in the HFR footprint area by means of the escape rate (Lai and Tel, 2011; Hernández-Carrasco et al., 2013). The main objective of this analysis was to investigate if in addition to favour cross-shelf transport, eddies favoured the local retention of shelf particles in the study area (see Rubio et al. 2018 for more details on this approach).

Finally, in order to offer further evidence on the origin of the particles that were transported by the eddy, backward Lagrangian connectivity maps were computed from 10 to 21 December, 2014. The maps were obtained integrating the trajectories of particles backward in time and then colouring each one depending on the boundary they crossed (Fig. 27). We used four boundaries: East, North, West and Coast, the last one corresponding to particles coming

from the coastal region (marked in red in Fig. 26). In these maps, it can be clearly observed that the eddy periphery was mostly composed by particles coming from the coastal region (in green) during the total integration time (15 days), demonstrating that the spatial distribution of Chl-a in the offshore area was largely produced by eddy-induced lateral stirring, transporting horizontally coastal waters to offshore regions.

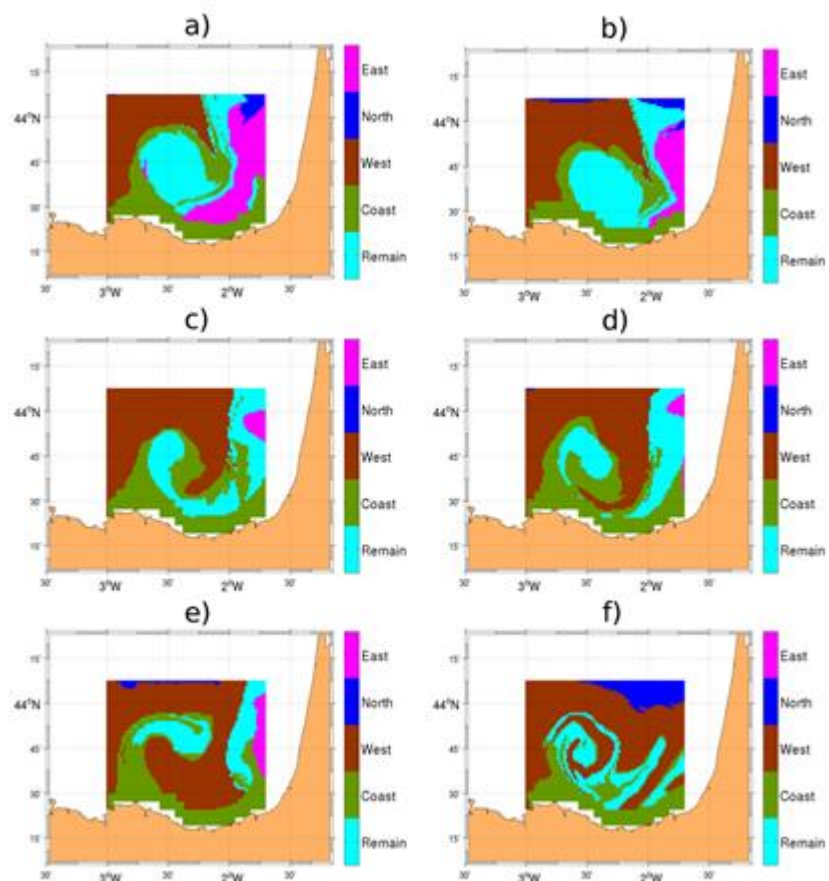


Figure 27. Snapshots of the backward connectivity Lagrangian maps corresponding to the same dates than the images plotted in Figure 26 (from 10 to 21 December, 2014). Green colour patches show regions where particles were coming from the coastal region. Particles coming from East, North, West boundaries are plotted in magenta, blue and brown, respectively. Particles remaining inside the area of study after the total time of integration (15 days) are coloured in cyan.

### 3.3.3.2. Application to fisheries (CNR-ISMAR)

Understanding the transport of fish larvae is relevant for a science based fishery management.

In this framework, computations of retention by currents measured by HFR have been performed in relevant coastal areas corresponding to spawning or nursery areas. The main step consists in estimating residence times from virtual trajectories computed from HF radar time series. This provides direct information on surface advected quantities. Since larvae typically move in the first 10-20 meters of the water column, though, these results should be



complemented when possible with water column information, to verify the degree of velocity correlation with depth.

The method has been tested and assessed within a study of sardine recruitment in the Adriatic Sea (Mediterranean Sea), focusing on the role of a well known recruitment area in the Manfredonia Gulf (Sciascia et al., 2018). The question of whether or not the Gulf is not only a nursery but also a spawning area has been addressed using data from a local HFR system (Cognati et al., 2019). Residence times have been computed and found to be relatively short, typically less than 5-6 days with std less than 4 days, and exceeding 10 days only during the month of October (Figure 28).

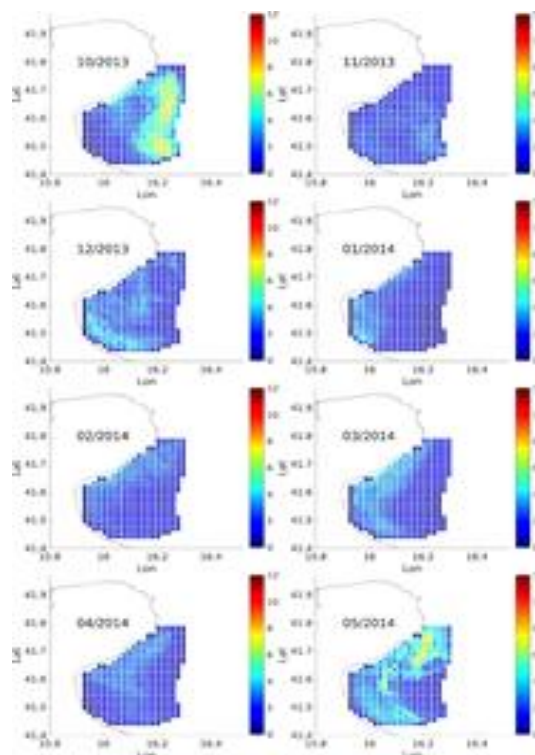


Figure 28: Monthly bootstrap estimates of average residence times (in days) of virtual particles advected in the HF radar velocity field and released within the boundaries of the Gulf of Manfredonia..

Comparison with velocity data from an ADCP in the Gulf during the winter spawning period indicate that in most cases the water column is primarily barotropic in the upper 20 m (correlation coefficient with the radar data in the range 0.95-0.75).

Overall, the residence times are short with respect to the Pelagic Larval Duration (PLD) of sardine larvae, which is estimated to be greater than 10 days, suggesting that local spawning and retention are not likely. Sardine larvae are likely to be advected to the Gulf from remote spawning areas, arriving in repeated pulses, as suggested also by drifter data and from otolith microstructure analysis.

### 3.3.3.3 Estimation of small scale convergence and potential impact on ecosystem dynamics (CNR-ISMAR)

Small, sub-mesoscale features in the ocean, such as eddies and jets in the range 100 m-10 km, are often characterized by high values of divergence/convergence and vorticity (Levy et al. 2012). Divergence/convergence areas induce significant vertical velocity, and therefore potential vertical transport of pollutants, such as microplastic and oil, nutrients, and biological quantities such as chlorophyll, larvae or eggs. As a consequence, the generation and evolution of sub-mesoscale structures are expected to have a significant impact on the dynamics of the marine ecosystem.

Sub-mesoscale observations are still relatively limited, because of the difficulties in collecting extensive measurements at the necessary high spatial and temporal resolution. HF radar data are well suited for this type of observations since they provide velocity maps at intervals of the order of 1 h and resolution of the order of 1 km, therefore resolving at least a good part of the sub-mesoscale range.

A method has been developed to use HF radar data to characterize and monitor the strength of sub-mesoscale features and the potential ecosystem impact. This is done computing vorticity and divergence from HF radar velocities in areas of particular interest, and then integrating them to obtain integral quantities that can be used as indexes. Their time series provide direct information on the variability of the sub-mesoscale flow.

The method has been tested in the Eastern Ligurian Sea (Mediterranean Sea), in an area situated in front of an important Marine Protected Area (Cinque Terre) and well known to be a favorable habitat for anchovies.

The investigation describes the evolution of ocean currents and wind during a 2-month period (October-November 2018), focusing on an extreme event occurred during the period October 25 - November 1. The interaction of sub-mesoscale with wind is still unknown (Thomas et al. 2013), and the results provide a very interesting test case given the high intensity of the wind.

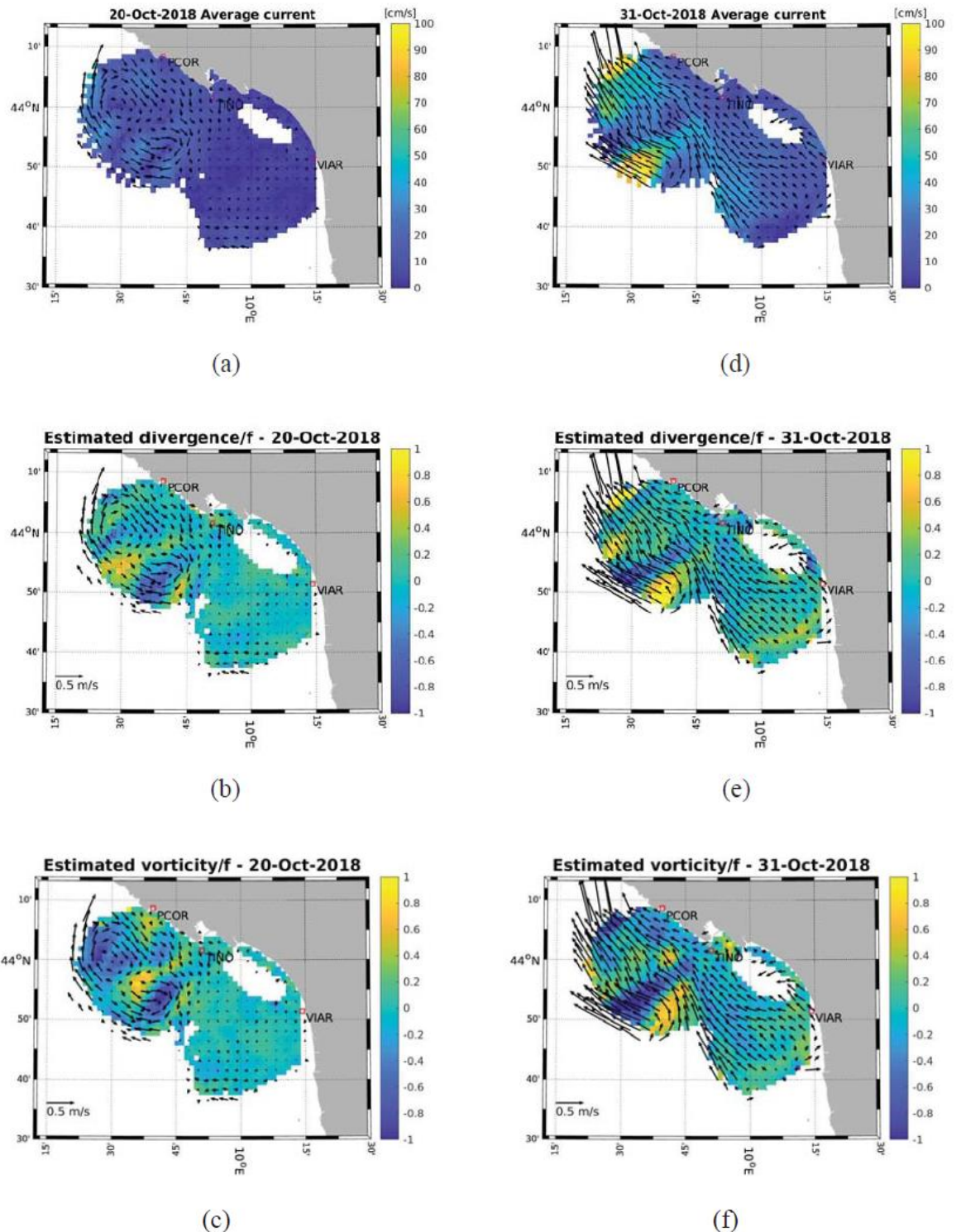


Figure 29: maps of daily average surface current (top panels), divergence and vorticity normalized by  $f$  (middle and bottom panels). Left (right) panels shows surface conditions before (after) the extreme wind event.

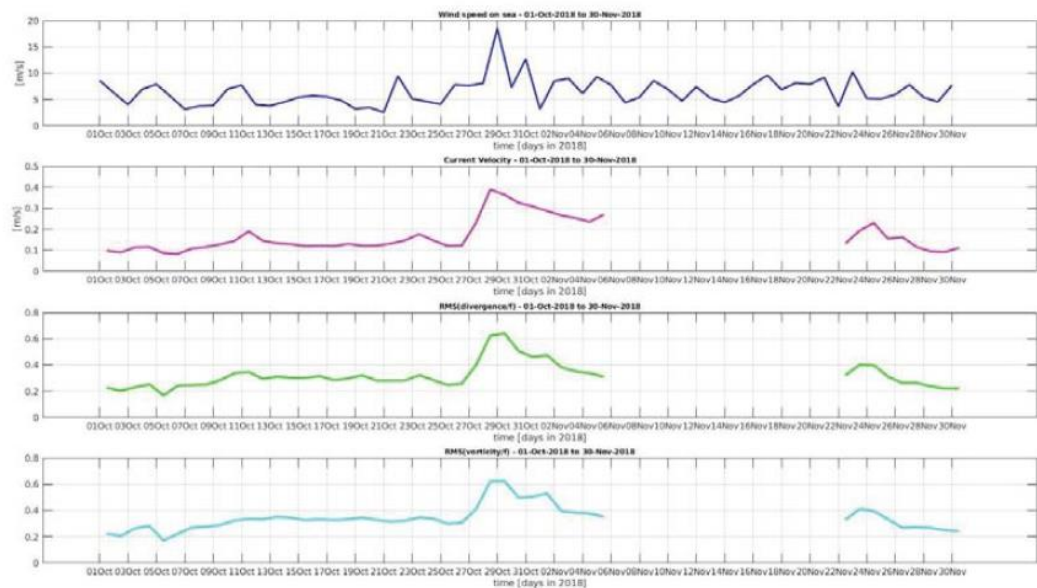


Figure 30: Time series of daily (top to bottom panel): average wind magnitude, average surface current magnitude, RMS of divergence and vorticity normalized by  $f$ .

Examples of velocity, divergence and vorticity maps from HF radar are shown in Figure 29, before (left panels) and after (right panel) the storm, while time series of the integral indexes are shown in Fig 30. As it can be seen from Figure 29, areas characterized by high velocities and divergence are wider and stronger after the storm, suggesting strong vertical velocities with potential high impact on the ecosystem. All the indexes in S2 show a strong increase and reach a maximum during the storm.

The results suggest that small scale marine “weather” can strongly impact transport both in the horizontal and in the vertical direction, and this could provide an important link to biological response. Indeed storms, because of the higher energy, transport and divergence, can act as triggering factors greatly influencing the ecosystem. Further studies specifically targeting the ecosystem response are necessary to quantitatively assess this important issue.

### 3.3.4 Improvement in short term prediction from HF radar data (IMEDEA UIB-CSIC, SOCIB, AZTI, KAUST)

The use of HF Radar data is increasing worldwide for operational oceanography, as it provides real-time coastal surface currents at high temporal and spatial resolution. For operational purposes, gap-filled fields are needed for Lagrangian applications as well as to forecast the trajectories for real applications. In the framework of Task 3.2, and in synergy with Task 3.7, investigations on short time prediction and data assimilation have been carried out.

An empirical real-time Short-Term Prediction (STP) system has been investigated and is in development in order to provide short term forecast (up

to 48 hours) of ocean currents from HF-Radar. The method, carried out in a collaboration between IMEDEA, SOCIB AZTI and L. Solabarrieta (Kaust), consists on the use of analogues of past fields. The system computes the trajectories of particles in the domain covered by the HF radar using the last 48 hours and it then searches for similar patterns in a pre-run data set of trajectories computed from a gap-filled set of OMA fields (see Figure 31). The method presented in EGU 2018 (see Solabarrieta et al. 2018) is applied to four years of hourly HF-Radar data and results show that the STP-system improves the persistence after 6 hours (See Figure 32). However, further analysis/developments are still needed to better understand the skills and limitations of the method.

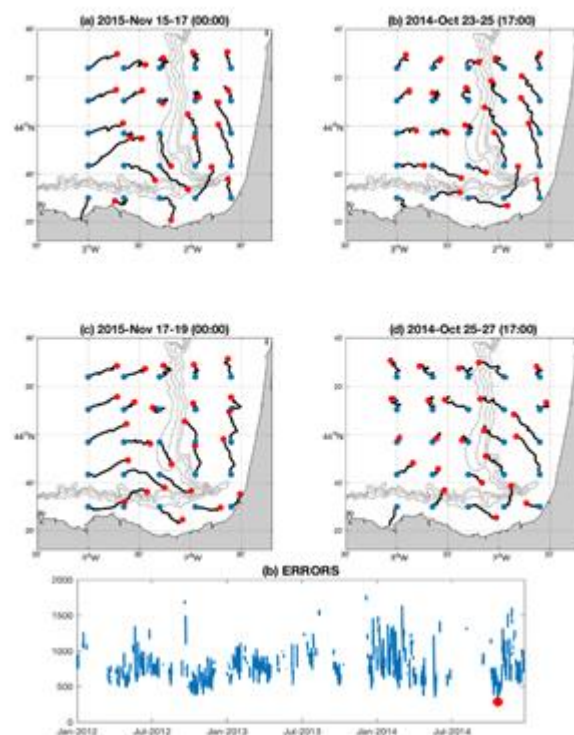


Figure 31. 17-Nov-2015 00:00 example of the developed methodology; (a) The past 48 hours of trajectories (b) The selected analogue (c) The real forecast for the target fields (“reference fields”) (d) the STP trajectories. From Solabarrieta et al. 2018.

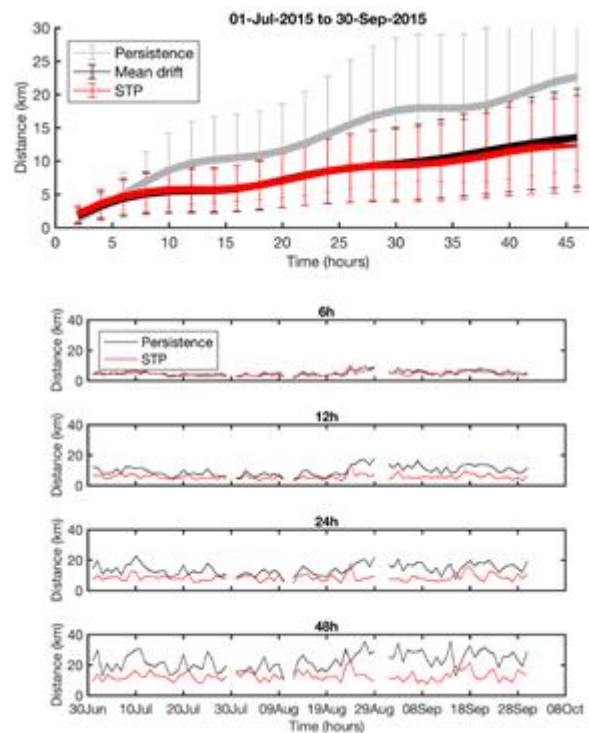


Figure 32 upper panel: Time evolution of the mean separation distances [km] between real and forecast trajectories using real and STP currents and the mean drift, for summer 2015. (Lower panels) Time evolution of the separation distances [km] between real and STP trajectories for various time gaps. From Solabarrieta et al. 2018.

### 3.3.5 Tests on assimilation of HF radar data (SMHI)

In most populated coastal regions, it is of great importance for society to be able to simulate drift trajectories of oil spills by making short-term ocean forecasts, and also for Search and Rescue operations. In order to improve forecast capabilities, the impact of assimilating HF radar data has been investigated, and tested on the Swedish west coast.

Two High-Frequency (HF) radars were deployed and operated on the Swedish west coast during autumn 2014 until late December 2015 (leased from CODAR, see the map in Figure 33). Due to a necessary change of frequency of the HF radars, the best quality from the system was acquired during the last ten months of operations (March to December 2015). Radial velocities from the two HF radar stations were used to calculate eastward and northward current components, which were subsequently assimilated into the ocean model NEMO-Nordic (Pemberton et al., 2017; Hordoir et al., 2019) which is currently the operational ocean forecasting model at SMHI. The data assimilation methods tested were 3D EnVar (Axell and Liu, 2016) and 4D EnVar (Axell and Liu, 2017), but only some 4D EnVar results will be shown here.

Figure 34 (a) shows the mean surface circulation in the overlapping area which is seen by both radar stations, where it is possible to calculate the full current

vectors from the radial velocities measured from the two stations. This example shows a monthly mean circulation for March 2015.

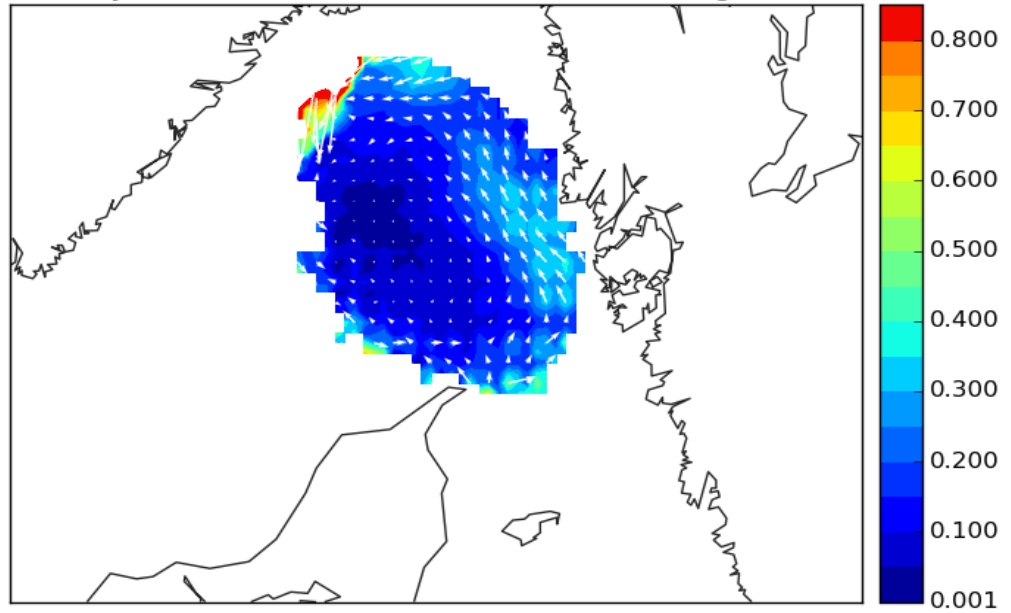
Figure 34 (b) shows the corresponding monthly mean circulation from a model simulation without data assimilation. The large-scale structure seems correct, but the northward current along the coast is a bit too strong and too narrow.

Figure 34 (c) shows the monthly mean circulation from the simulation with 4D EnVar data assimilation, and Figure 34 (d) shows the mean data assimilation increment. From these figures we see that the data assimilation tries to slow down the northward coastal current of the Swedish coast, while making it wider in accordance with the observations in Figure 34 (a)

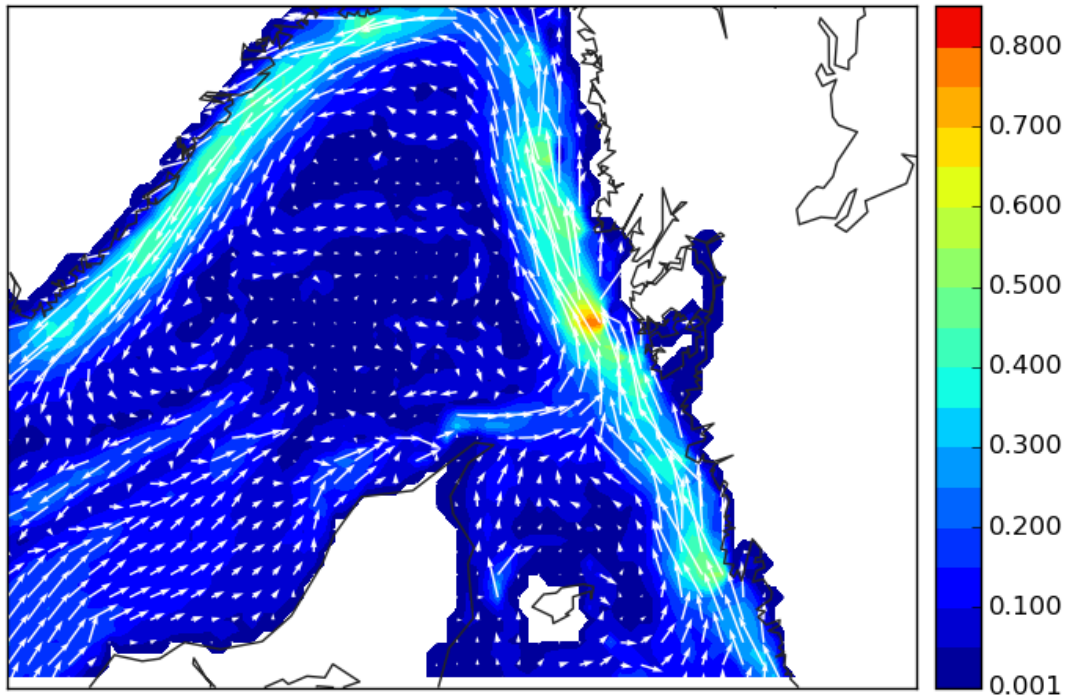


Figure 33. Locations of the two HF radar stations on the Swedish west coast, that were leased from CODAR.

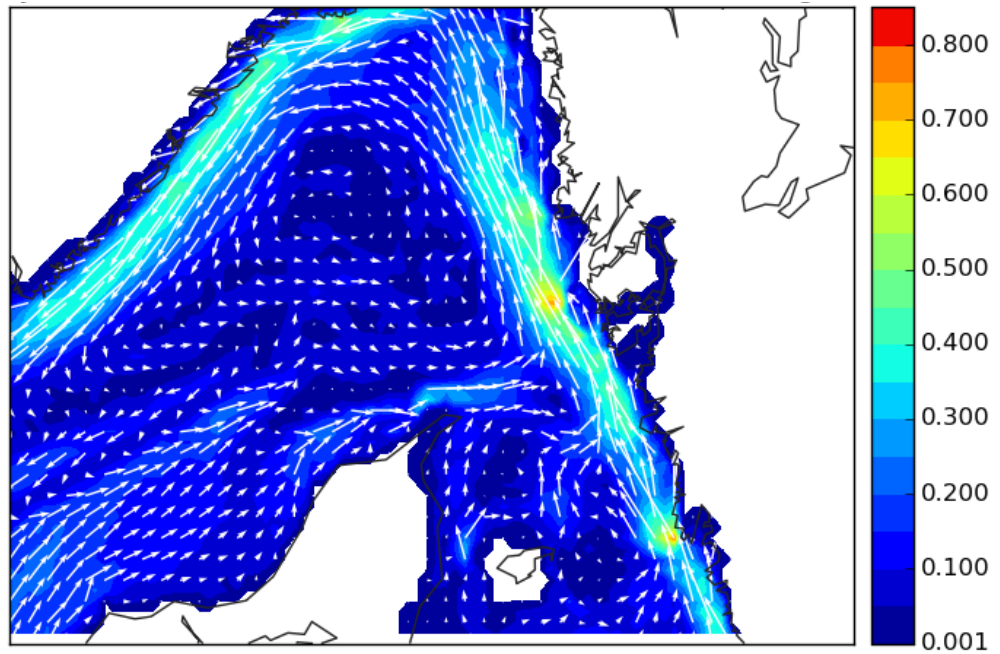
Monthly Mean Observed Surface Currents during 2015-03



(a)

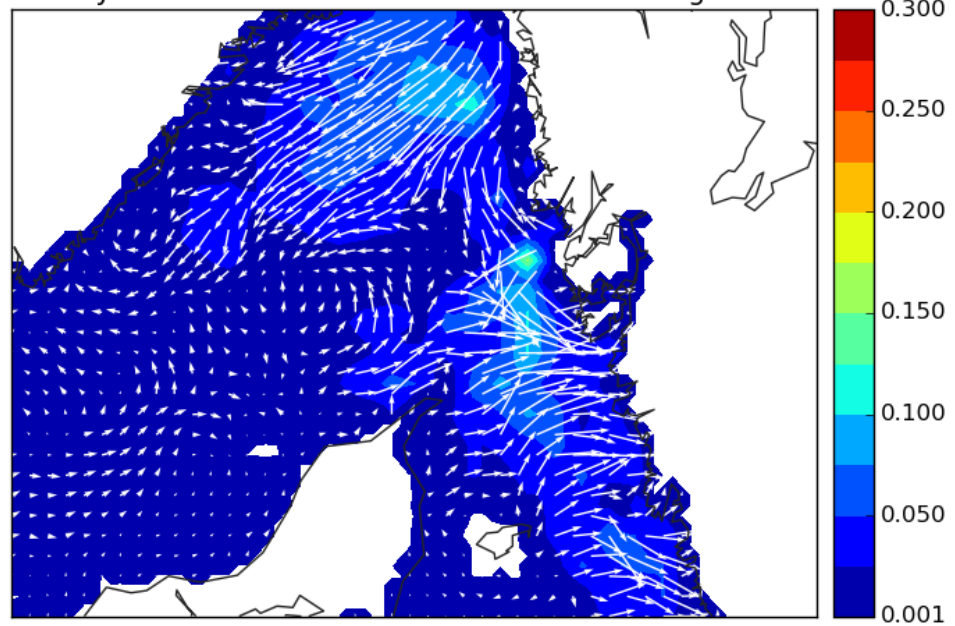


(b)



(c)

Monthly Mean Surface Currents increments during 2015-03



(d)

Figure 34. Surface mean currents according to (a) HF radar, (b) a simulation without data assimilation, (c) a simulation with data assimilation, and (d) the mean data assimilation increment. All figures show mean data for March 2015.



To conclude, data assimilation using two HF radars on the Swedish west coast is indeed possible, but the difference compared to the free simulation is limited, given that the HF radar data coverage in terms of velocity vectors is relatively small with respect to the area of interest. In contrast, the measured radial velocities from the two stations cover a much larger area. Hence, a goal for the future is to prepare the data assimilation system for handling radial velocities directly. It is possible that the impact of the data assimilation will increase as a result. In addition, assimilation of the temperature-salinity structure may further constrain the data assimilation and thus improve the results. Finally, the HF radar system was only leased for a short period during 2014-2015 and no Swedish system exists today (albeit a Norwegian system has been set up in southern Norway). Hence, a future goal is to start setting up a system along the coasts for future use in operational forecasting.





## 4. Conclusions

Deliverable D3.4 provides reporting on all the methodological improvements and assessments developed in the framework of Task 3.2. An impressive suite of new tools is presented, and their impact on the use of HF radars is discussed. HF radars were a relatively new monitoring technology in Europe at the beginning of JERICO-NEXT, and they have greatly benefit from the joint effort of the various WPs within the project (WP3, WP2, WP5). HF radars are today a vital and growing part of the observing system in Europe, and their data is now integrated in all the main platforms such as CMEMS, SDC and EMODNET. WP3 and in particular Task 3,2, have greatly contributed to this development, through methodological development and testing.

The results presented in D3.4 are focused on 3 main aspects summarized as follows

- 1) The quality of current retrievals has been investigated, and methods to improve their QC have been developed and tested. Two main aspects have been investigated. On the one side, a focused scientific investigation has been performed on how to quantify accuracy in the important and still unknown case of high current subgrid variability. Results have been tested in terms of “accuracy” parameter and threshold, in the case of WERA systems in the German Bight. This is a particularly challenging environment characterized by shallow and highly variable topography and strong tidal variability. The approach provides general methodological indications that can be applied to different situations. The other aspect that has been finalized, is the scientific support provided to the interoperability effort carried out in the framework of WP5, in particular in terms of common QC tests proposed for the European community. A first set of QC tests have been proposed in D5.13, and they have been further investigated and refined within Task 3.2 thanks to an international collaboration including also US and Australian scientists. This collaborative work led to the advanced QC version delivered in D5.14.
- 2) Methods to guide the design of HF radar networks have been completed. The proposed methodology allows to identify gaps and define priorities for planning the installation of new HF radar stations. The geographical distribution of the main requirements and the capabilities of the HF radar network have been combined to assess the benefits of different scenarios. A demonstration have been performed in a pilot area characterizing different scenarios and allowing a cost benefit analysis. Following this methodology, deeper analysis could be performed at Regional level detailing the information on weighted requirements (depending on socio-economical priorities) and adding data on vulnerability (protected area, habitats). In addition, a tool for integrating information on the





variability of the ocean processes has been tested. Further developments will allow to integrate key information for assessing also the impact for data assimilation configurations, considering the installation of medium and standard range radars.

- 3) A number of new products have been implemented for the analyses of HF radar and their use in practical application, as detailed below.

Blending of HF radar data with ADCP and glider data. This is a very important aspect for future integration of the observing system, especially for the computation of transport of pollutant and biological quantities due to ocean currents. HF radar data, in fact, provide current velocity information over extended areas, but only at the surface (approximately within the first meter of water), while ADCP and gliders provide information throughout the water column but only in restricted areas. Various aspects of the problem have been tested. Blending with ADCPS have been investigated considering two different methods applied to model synthetic data in the BoB. Potentials and limitations of the two methods have been quantified and highlighted, providing a basis for future applications also in other areas. For gliders, that measure only the geostrophic component of velocity, a method has been develop to first separate geostrophic and wind driven components using HF radar data. The method has been tested in the NW Med, and first blending tests with gliders have been performed with positive results.

Gap filling. HF radar data can have gaps both spatially and temporally due to various technical and environmental reasons, and being able to fill them is very important especially to compute trajectories and transport in many applications. Various methods have been tested in BoB and NW Med, and a new methodology has been implemented and tested in the BoB. Results provide guidance for a number of applications.

Flow characterization methods for biological applications. Two threads have been investigated. The first one deals with Lagrangian method to quantify flow transport and retention, and their potential impact on phytoplankton or larval transport. A general methodology has been tested in the BoB and an example of application to fishery management has been performed in the Adriatic Sea. The other aspect deals with the introduction of indexes of divergence and vertical velocities in the flow, that can influence ecosystem response. A method has been introduced and tested in the NW Med, Both threads have great potential of being applied in practical applications using HF radar data

Improvements in flow and transport predictability. All the methodologies above





are typically applied in hindcast mode, but transitioning to forecast mode is of course of great importance for all the applications. The question of how to improve forecast using HF radar data has been addressed using two different approaches. The first one, tested in the BoB is focused on short term forecast (48 h) of particle trajectories, based on the analysis of historical data. The second one instead, applied along the Swedish coast, relies on data assimilation methods to improve flow forecast. Advantages, limitations and future directions of both methods are discussed,

Overall, an impressive suite of new tools have been investigated and tested in key areas of the European seas. An important point to be noticed is that the results not only provide a solid basis for future applications, but also provide important indications on open issues and existing gaps in our present knowledge and observing capabilities, while indicating possible roads for improvement. As an example, the results on HFR based Lagrangian methodologies to quantify transport indicate that for biological applications several complementary information are needed. They include physical information on the water column in order to provide 3d transport, and biogeochemical information to quantify the ecosystem response. Steps toward this integration are provided by the blending results, but further efforts are needed especially regarding the integration with biogeochemical data. Also, results on the accuracy of velocity retrievals point out to the fact that indeed there are technical and environmental limits that have to be taken into account when analysing HFR data, and specific tools have to be used to evaluate them. Finally, the results on assimilation point out to the limits of the present HFR coverage and indicate the importance of improving methods based on radial velocities, given their extended range.





## 5. Annexes and references

- Axell, L. and Liu, Y. (2016). Application of 3-D ensemble variational data assimilation to a Baltic Sea reanalysis 1989-2013, *Tellus A* 2016, 68, 24220, <http://dx.doi.org/10.3402/tellusa.v68.24220>.
- Axell, L. and Liu, Y. (2017). Ensemble-based data assimilation of observations into NEMO-Nordic, 8 th EuroGOOS Conference, Bergen, 3-5 October 2017.
- Beckers, J. M. and Rixen, M.: EOF calculations and data filling from incomplete oceanographic datasets, *J. Atmos. Ocean. Tech.*, 20, 1839–1856, [https://doi.org/10.1175/1520-0426\(2003\)020<1839:ECADFF>2.0.CO;2](https://doi.org/10.1175/1520-0426(2003)020<1839:ECADFF>2.0.CO;2), 2003.
- Beckers, J.-M., Barth, A., Tomazic, I., and Alvera-Azcárate, A.: A method to generate fully multi-scale optimal interpolation by combining efficient single process analyses, illustrated by a DINEOF analysis spiced with a local optimal interpolation, *Ocean Science*, 10, 845–862, <https://doi.org/10.5194/os-10-845-2014>, 2014.
- Berta, M., Bellomo, L., Griffa, A., Magaldi, M. G., Molcard, A., Mantovani, C., Gasparini, G. P., Marmain, J., Vetrano, A., Béguery, L., Borghini, M., Barbin, Y., Gaggelli, J., and Quentin, C. (2018), Wind-induced variability in the Northern Current (northwestern Mediterranean Sea) as depicted by a multi-platform observing system, *Ocean Sci.*, 14, 689-710. <https://doi.org/10.5194/os-14-689-2018>
- Boffetta, G., Celani, A., Cencini, M., Lacorata, G., and Vulpiani, A.: Non-asymptotic properties of transport and mixing, *Chaos*, 10, 50–60, <https://doi.org/10.1063/1.166475>, 2000.
- Corgnati, L. P., C. Mantovani, A. Griffa, M. Berta, P. Penna, P. Celentano, L. Bellomo, D.F. Carlson, R. D’Adamo (2019), "Implementation and Validation of the ISMAR High-Frequency Coastal Radar Network in the Gulf of Manfredonia (Mediterranean Sea)," in *IEEE Journal of Oceanic Engineering*, vol. 44, no. 2, pp. 424-445. doi: 10.1109/JOE.2018.2822518
- D’Ovidio, F., Fernández, V., Hernández-García, E., and López, C., 2004. Mixing structures in the Mediterranean sea from Finite-Size Lyapunov Exponents, *Geophys. Res. Lett.*, 31, L17203, doi:10.1029/2004GL020328.
- Dick, S., E. Kleine, S. Müller-Navarra, H. Klein, and H. Komo, The Operational Circulation Model of BSH (BSHcmod), Model Description and Validation, Tech. Rep. 29/2001, BSH, 2001.
- Esnaola, G., Sáenz, J., Zorita, E., Lazure, P., Ganzedo, U., Fontán, A., Ibarra-Berastegi, G., and Ezcurra, A.: Coupled airsea interaction patterns and surface heat-flux feedback in the Bay of Biscay, *Journal of Geophysical Research-Oceans*, 117, <https://doi.org/10.1029/2011JC007692>, 2012.
- Fredj, E., Roarty, H., Kohut, J., Smith, M., and Glenn, S.: Gap Filling of the Coastal Ocean Surface Currents from HFR Data: Application to the Mid-Atlantic Bight HFR Network, *J. Atmos. Ocean. Tech.*, 33, 1097–1111, <https://doi.org/10.1175/JTECHD-15-0056.1>, 2016.
- Ganzedo, U., Alvera-Azcárate, A., Esnaola, G., Ezcurra, A., and Sáenz, J.: Reconstruction of sea surface temperature by means of DINEOF: a case study





- during the fishing season in the Bay of Biscay, *International Journal of Remote Sensing*, 32, 933 – 950, <https://doi.org/10.1080/01431160903491420>, 2011.
- Garcia, D., 2010: Robust smoothing of gridded data in one and higher dimensions with missing values. *Comput. Stat. Data Anal.*, 54, 1167–1178, doi:10.1016/j.csda.2009.09.020.
- Haller, G., Yuan, G., 2000. Lagrangian coherent structures and mixing in two-dimensional turbulence, *Physica D*, 147, 352–370.
- Hernández-Carrasco, I., Lopez, C., Hernández.-Garcia, E., Turiel A., 2011. How reliable are finite-size Lyapunov exponents for the assessment of ocean dynamics? *Ocean Modelling*, 36(3-4), 208 – 218, doi:10.1016/j.ocemod.2010.12.006.
- Hernández-Carrasco, I., López, C., Orfila, A., Hernández-García E., 2013. Lagrangian transport in a microtidal coastal area: the bay of Palma, island of Mallorca, Spain, *Non-linear Processes in Geophysics*, 20(5), 921–933, doi:10.5194/npg-20-921-2013.
- Hernández-Carrasco, I., Solabarrieta, L., Rubio, A., Esnaola, G., Reyes, E., and Orfila, A.: Impact of HF radar current gap-filling methodologies on the Lagrangian assessment of coastal dynamics, *Ocean Sci.*, 14, 827-847, <https://doi.org/10.5194/os-14-827-2018>, 2018.
- Hordoir, R., Axell, L., Höglund, A., Dieterich, C., Fransner, F., Gröger, M., Liu, Y., Pemberton, P., Schimanke, S., Andersson, H., Ljungemyr, P., Nygrem P., Falahat, S., Nord, A., Jönsson, A., Lake, I., Döös, K., Hieronymous, M., Dietze, H., Löptien, U., Kuznetsov, I., Westerlund, A., Tuomi, L., Haapala, J. (2019). Nemo-Nordic 1.0: a NEMO-based ocean model for the Baltic and North seas – research and operational applications, *eosci. Model Dev.*, 12, 363–386, 2019 <https://doi.org/10.5194/gmd-12-363-2019>.
- Jordà, G., Sanchez-Roman, A., and Gomis, D. (2016). Reconstruction of transports through the Strait of Gibraltar from limited observations. *Clim. Dynam*, 1–15, doi:10.1007/s00382-016-3113-8
- Joseph, B. and Legras, B.: Relation between Kinematic Boundaries, Stirring, and Barriers for the Antarctic Polar Vortex, *J. Atm. Sci.*, 59, 1198–1212, [https://doi.org/10.1175/1520-0469\(2002\)059<1198:RBKBSA>2.0.CO;2](https://doi.org/10.1175/1520-0469(2002)059<1198:RBKBSA>2.0.CO;2), 2002.
- Kaplan A, Kushnir Y, Cane MA (2000) Reduced space optimal interpolation of historical marine sea level pressure: 1854–1992. *J Clim* 13:2987–3002
- Kaplan D. M., Lekien F., 2007. Spatial interpolation and filtering of surface current data based on open-boundary modal analysis. *J. Geophys Res.-Oceans* 112(C12). doi:10.1029/2006JC003984
- Kohonen, T.: Self-Organized Formation of Topologically Correct Feature Maps, *Biol. Cybern.*, 43, 59–69, 1982.
- Kohonen, T.: Self-Organizing Maps, 2nd edn., Springer, Heidelberg, Germany, 1997.
- Lévy, M., R. Ferrari, P. J. S. Franks, A. P. Martin, and P. Rivière (2012), Bringing physics to life at the submesoscale, *Geophys. Res. Lett.*, 39, L14602, doi:10.1029/2012GL052756.
- Pemberton, P., Löptien, U., Hordoir, R., Höglund, A., Schimanke, S., Axell, L., and Haapala, J. (2017). Sea-ice evaluation of NEMO-Nordic 1.0: a NEMO–LIM3.6-based ocean–sea-ice model setup for the North Sea and Baltic Sea, *Geoscientific Model Development*, 10, 3105-3123, <https://doi.org/10.5194/gmd-10-3105-2017>.





- Rubio, A., Caballero, A., Orfila, A., Hernández-Carrasco, I., Ferrer, L., González, M., Solabarrieta, L., and Mader, J.: Eddy-induced cross-shelf export of high Chl-a coastal waters in the SE Bay of Biscay, *Remote Sensing of Environment*, 205, 290–304, <https://doi.org/10.1016/j.rse.2017.10.037>, 2018.
- Sciascia, R., Berta, M., Carlson, D. F., Griffa, A., Panfili, M., La Mesa, M., Corgnati, L., Mantovani, C., Domenella, E., Fredj, E., Magaldi, M. G., D'Adamo, R., Paziienza, G., Zambianchi, E., and Poulain, P.-M. (2018), Linking sardine recruitment in coastal areas to ocean currents using surface drifters and HF radar. A case study in the Gulf of Manfredonia, Adriatic Sea, *Ocean Sci.*, 14, 1461–1482. <https://doi.org/10.5194/os-14-1461-2018>
- Shadden, S. C., Lekien, F., Marsden, J. E., 2005. Definition and properties of Lagrangian coherent structures from finite-time Lyapunov exponents in two dimensional aperiodic flows, *Physica D*, 212, 271–304
- Solabarrieta, L., Frolov, S., Cook, M., Paduan, J., Rubio, A., González, M., Mader, J., Charria, G., 2016. Skill assessment of HF radar-derived products for lagrangian simulations in the Bay of Biscay. *J. Atmos. Oceanic Technol.*, 33, 2585–2597, doi: 10.1175/JTECH-D-16-0045.1.
- Solabarrieta, L., Orfila, A., Rubio, A., Hernández-Carrasco, I., Mader, Jones, B.J. Exploring a new Lagrangian based Short Term Prediction methodology for HF Radar currents. , *Geophysical Research Abstracts Vol. 20*, EGU2018-17858. EGU General Assembly 2018. Oral.
- Thomas, L. N., Tandon, A. and Mahadevan, A. (2013). Submesoscale Processes and Dynamics. In *Ocean Modeling in an Eddy Regime* (eds M. W. Hecht and H. Hasumi). doi:10.1029/177GM04
- Volpe, G., Nardelli, B. B., Cipollini, P., Santoleri, R., and Robinson, I. S.: Seasonal to interannual phytoplankton response to physical processes in the Mediterranean Sea from satellite observations, *Remote Sensing of Environment*, 117, 223–235, <https://doi.org/10.1016/j.rse.2011.09.020>, *remote Sensing of Urban Environments*, 2012.

